Icarus 315 (2018) 124–145

Contents lists available at ScienceDirect

Icarus

journal homepage: www.elsevier.com/locate/icarus

Breaking up is hard to do: Global cartography and topography of Pluto's mid-sized icy Moon Charon from New Horizons

Paul Michael Schenk[a,*], Ross A. Beyer[b,c], William B. McKinnon[d], Jeffrey M. Moore[b], John R. Spencer[e], Oliver L. White[b], Kelsi Singer[e], Orkan M. Umurhan[b], Francis Nimmo[f], Tod R. Lauer[g], William M. Grundy[h], Stuart Robbins[e], S. Alan Stern[e], Harold A. Weaver[i], Leslie A. Young[e], K. Ennico Smith[b], Cathy Olkin[e], the New Horizons Geology and Geophysics Investigation Team

[a] *Lunar and Planetary Institute, 3600 Bay Area Blvd., Houston TX 77058, USA*
[b] *NASA Ames Research Center, Moffett Field, CA, USA*
[c] *Sagan Center at the SETI Institute, Mountain View, CA, USA*
[d] *Department Earth and Planetary Sciences, Washington Univ. St. Louis, St. Louis, MO, USA*
[e] *Southwest Research Institute, 1050 Walnut St., Suite 300, Boulder, CO, USA*
[f] *University of California at Santa Cruz, Santa Cruz, CA, USA*
[g] *National Optical Astronomy Observatory, Tucson, AZ, USA*
[h] *Lowell Observatory, Flagstaff, AZ, USA*
[i] *Johns Hopkins University, Applied Physics Laboratory, Laurel, MD, USA*

A B S T R A C T

The 2015 New Horizons flyby through the Pluto system produced the first high-resolution topographic maps of Pluto and Charon, the most distant objects so mapped. Global integrated mosaics of the illuminated surface of Pluto's large icy moon Charon have been produced using both framing camera and line scan camera data (including four-color images at up to 1.47 km pixel scales), showing the best resolution data at all areas of the surface. Digital elevation models (DEMs) with vertical precisions of up to ~0.1 km were constructed for ~40% of Charon using stereo imagery. Local radii estimates for the surface were also determined from the cartographic control network solution for the LORRI framing camera data, which validate the stereo solutions. Charon is moderately cratered, the largest of which is ~250-km across and ~6 km deep. Charon has a topographic range over the observed hemisphere from lowest to highest of ~19 km, the largest topographic amplitude of any mid-sized icy body (including Ceres) other than Iapetus. Unlike Saturn's icy moons whose topographic signature is dominated by global relaxation of topography and subsequent impact cratering, large-scale tectonics and regional resurfacing dominate Charon's topography. Most of Charon's encounter hemisphere north of the equator (Oz Terra) is broken into large polygonal blocks by a network of wide troughs with typically 3–6 km relief; the deepest of these occur near the illuminated pole and are up to 13 km deep with respect to the global mean radius, the deepest known surfaces on Charon. The edge of this terrain is defined by large tilted blocks sloping ~5° or so, the crests of which rise to 5 or 6 km above Charon mean, the highest known points on Charon. The southern resurfaced plains, Vulcan Planitia, consist of rolling plains, locally fractured and pitted, that are depressed ~1 km below the mean elevation of the disrupted northern terrains of Oz Terra that comprise much of the northern hemisphere (but ~2–2.5 km below the surfaces of the blocks themselves). These plains roll downward gently to the south with a topographic range of ~5 km. The outer margins of Vulcan Planitia along the boundary with Oz Terra form a 2-3-km-deep trough, suggesting viscous flow along the outer margins. Isolated massifs 2–4 km high, also flanked by annular moats, lie within the planitia itself. The plains may be formed from volcanic resurfacing of cryogenic fluids, but the tilted blocks along the outer margins and the isolated and tilted massifs within Vulcan Planitia also suggest that much of Charon has been broken into large blocks, some of which have been rotated and some of which have foundered into Charon's upper "mantle", now exposed as Vulcan Planitia, a history that may be most similar to the disrupted terrains of Ariel.

1. Introduction

The New Horizons spacecraft passed through the Pluto system on 14 July 2015, and executed a series of observations designed to map the composition, surface morphology, and topography of both Pluto and its largest moon, Charon (Stern et al., 2015; Moore et al., 2016), the topic of this report. Charon is comparable in size, density and bulk composition to the 11 classical mid-sized satellites of Saturn and Uranus, which are dominated by mixed ice and rock composition. These include Mimas, Enceladus, Dione, Tethys, Rhea, Iapetus, Miranda, Ariel, Umbriel, Titania and Oberon. These bodies exhibit a rich variety of geologic processes (e.g., Croft and Soderblom, 1991; Schenk et al., 2018a)

* Corresponding author.
E-mail address: schenk@lpi.usra.edu (P.M. Schenk).

https://doi.org/10.1016/j.icarus.2018.06.010
Received 13 September 2017; Received in revised form 5 June 2018; Accepted 6 June 2018
Available online 03 July 2018

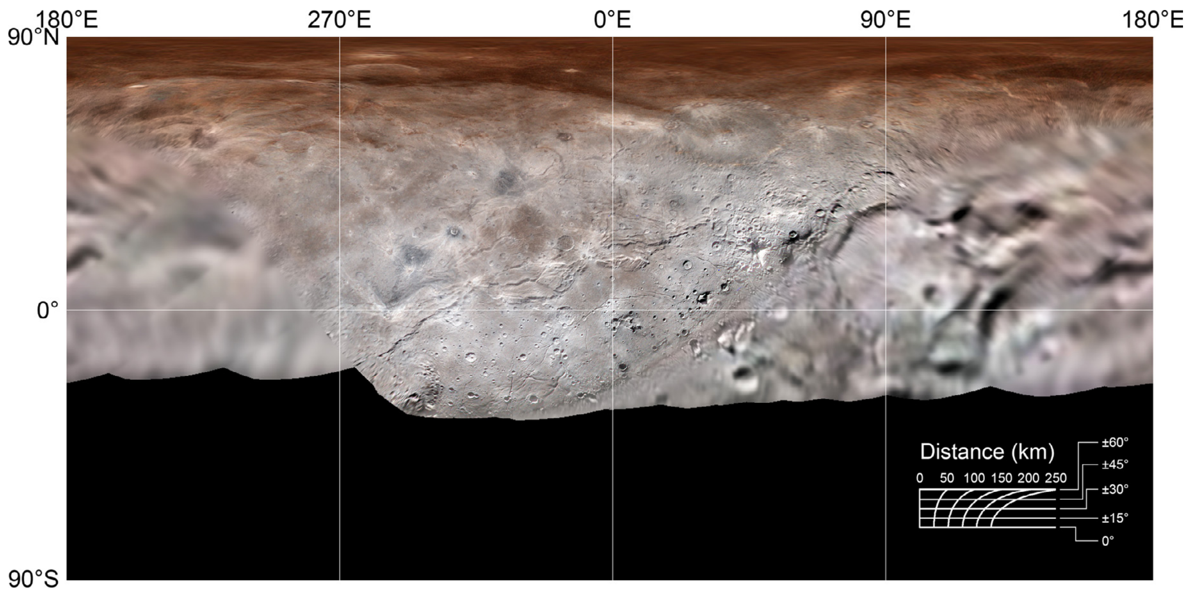

Fig. 1. Global image mosaic of Charon, produced at 300 m/pixel. Dark areas were unilluminated during the 2015 encounter. The encounter hemisphere is in map center, with approach imaging to the left starting at ~60 km/pixel resolution and increasing in quality to the west (left). Global cylindrical map from −180° to + 180°E is centered on 0° longitude. The color version of this mosaic uses MVIC 875, 625, and 475 nanometers filter images. Global 4-color mosaic of Charon at 300 m/pixel. MVIC filters used here are centered on 875, 625, and 475 nanometers, displayed in the red, green, and blue color channels, respectively. Dark areas were unilluminated during the 2015 encounter. The encounter hemisphere is in map center, with approach imaging to the left starting at ~60 km/pixel resolution and increasing in quality to the west (left). Global cylindrical map from −180° to +180°E is centered on 0° longitude. (For interpretation of the references to color in this figure legend, the reader is referred to the web version of this article.)

from tectonic fracturing to volcanic resurfacing by several possible ice phases as well as a variety of exogenic alteration processes. These icy bodies formed and evolved in close proximity to large planetary bodies, which have influenced their geology through tidal heating and deformation (Collins et al., 2010). Hence there was considerable interest in how Charon evolved being a satellite of a much smaller planetary body, namely Pluto.

Charon is also very similar in size and density to the ice-rich solar-orbiting dwarf planet Ceres (e.g., Buczkowski et al., 2016), and both bodies appear to have ammonia-enriched surface (and likely internal) compositions (e.g., Grundy et al., 2016a; Dalle Ore et al., 2018; Cook et al., 2018; De Sanctis et al., 2016). While Ceres (like Charon) has likely been in solar orbit for some time, its unusual surface composition has led to speculation that Ceres is a possible escapee of the Kuiper Belt (McKinnon, 2012) [or the Jupiter-Saturn region (J. Castillo-Rogez, pers. comm.)] and a possible cousin to Pluto or Charon.

As a class, impact and other geologic processes on the icy mid-sized bodies also occur under lower surface gravity and (usually) lower heat budgets than typically observed on the larger icy moons such as Ganymede, Europa, and Triton, or on Pluto, and as such Pluto is discussed in a separate report (Schenk et al., 2018b). Happily, Charon proved to be a geologically complex world disrupted by tectonism and volcanism (Moore et al., 2016; Beyer et al., 2017; Robbins et al., 2017). Here, using cartographic and topographic mapping products from New Horizons we document and describe the regional and global topographic characteristics of Charon, and compare them with other similar-sized icy bodies.

2. Cartographic mapping

2.1. Global mapping coverage and base map production

The New Horizons mapping strategies for Charon were essentially the same in character as those for Pluto (Schenk et al., 2018b), leading to the production of similar mapping data sets for the two bodies. Here we summarize those mapping strategies and data sets for Charon but refer the reader to the Pluto report for technical details. The cartographic and stereo imaging campaign was conducted by the Long-Range Reconnaissance Imager (LORRI, Cheng et al., 2008) and the Multi-spectral Visible Imaging Camera (MVIC) on the Ralph instrument (Reuter et al., 2008), supplemented by LEISA multispectral mapping (e.g., Grundy et al., 2016a; Dalle Ore et al., 2018), with the best mapping and stereo imaging on the illuminated Pluto-facing hemisphere of Charon (Figs. 1–4).

We define longitude and latitude on Charon according to the right hand rule and follow the recommendations of Zangari (2015). Charon's positive pole is defined by Archinal et al. (2011a, b) and points in the direction of the angular momentum vector. Charon's prime or 0° meridian is the sub-Pluto longitude. Consequently, an observer at infinity who sees Pluto at a sub-observer longitude of 180°, will see a sub-observer longitude of 0° on Charon (and thus New Horizons imaged the anti-Charon hemisphere of Pluto and the sub-Pluto hemisphere of Charon). Informally, we refer to the positive pole direction as “North,” and to the direction of increasing longitude as “East”.

During approach, LORRI imaging of Charon (and Pluto) was acquired approximately every 15° of longitude during the last Pluto/Charon day (6.4 Earth days) before encounter, thereby providing continuous longitudinal mapping (Fig. 1). Pixel scales improved toward the west from ~35 to 0.15 km/pixel as Charon rotated under the approaching spacecraft (Fig. 2a). Terrains south of −38° were in darkness due to polar obliquity at the time of encounter. In order to produce a global map of Charon with minimal viewing angle distortions and best resolution at each point on the surface, all imaging data at emission angles > 75° (and >70° for low resolution images) and all data at incidence angles > 88° (and >85° for low resolution images) were removed (Fig. 2c, d). The resulting global map product shows the illuminated surface of Charon North of −35° latitude. The global Charon base map (Fig. 1) and topographic DEM (Fig. 3) were constructed in the same manner and using the same parameters as for Pluto (Schenk et al., 2018b) except that the encounter hemisphere mapping area data are approximately a factor of two lower in resolution due to the greater distance of Charon at closest approach. The best hemispheric MVIC scan was at ~0.6 km/pixel, and the highest resolution LORRI 5 × 1 mosaic along the center of the hemisphere was at ~0.15 km/pixel

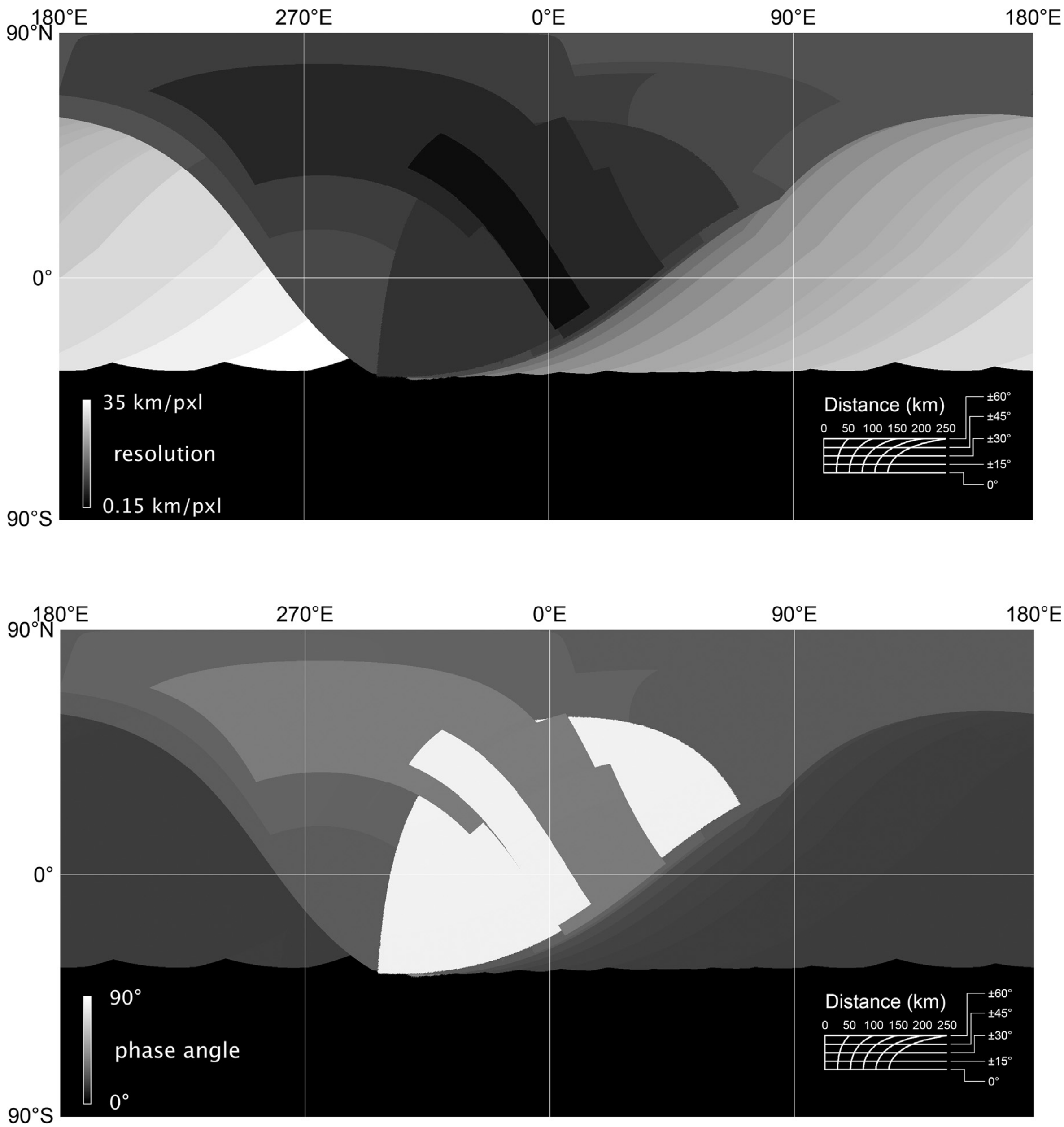

Fig. 2. Global maps illustrating the pixel scale, phase angle, incidence angle, emission angle associated with the panchromatic base map of Charon in Fig. 1. Global cylindrical map from −180° to +180°E is centered on 0° longitude.

(both part of the C_MVIC_LORRI_CA observation).

The default pixel scales of the Charon base maps were chosen to be 0.3 km; the best ~0.15 km/pixel LORRI 5 × 1 mosaic strip was small in area and also noisier than most other images due to short exposure times and this image strip was smoothed to an effective resolution of 0.3 km/pixel for mapping purposes. Images used for mapping in the non-encounter hemisphere were obtained with LORRI. The LORRI point spread function has a full width at half maximum (FWHM) of ~2 pixels, which meets its specifications (Cheng et al., 2008), but can cause slight but noticeable blurring. This can be improved through Lucy (1974) - Richardson (1972) deconvolution, and the LORRI images for this hemisphere were processed in this way in order to improve sharpness.

2.2. Control network for Charon

Accurate positional referencing of surface features and derivation of topography on Charon from stereo images requires precision knowledge of camera pointing and spacecraft position. Spacecraft position data were supplied by the New Horizons navigation team (https://naif.jpl.nasa.gov/pub/naif/pds/data/nh-j_p_ss-spice-6-v1.0/nhsp_1000/). Camera pointing information (SPICE kernels after Acton et al., 2011) were updated by PS and RB for the entire New Horizons image library over the final Charon 6.4-day rotation approach phase, as they were for Pluto. Cartographic control utilized Integrated Software for Imagers and Spectrometers (ISIS3) software (USGS, 2017). The method requires selection of tie points linking overlapping resolvable images at numerous points on the surface, and then performing bundle adjustment (via the ISIS jigsaw program) to the camera pointing vectors for all images to minimize the differences in the computed surface coordinates for all images associated with each tie point in the control network, in images where each point can be resolved.

As on Pluto, existing ISIS software did not permit the use of framing camera images (LORRI) and line-scan (MVIC) images in the same

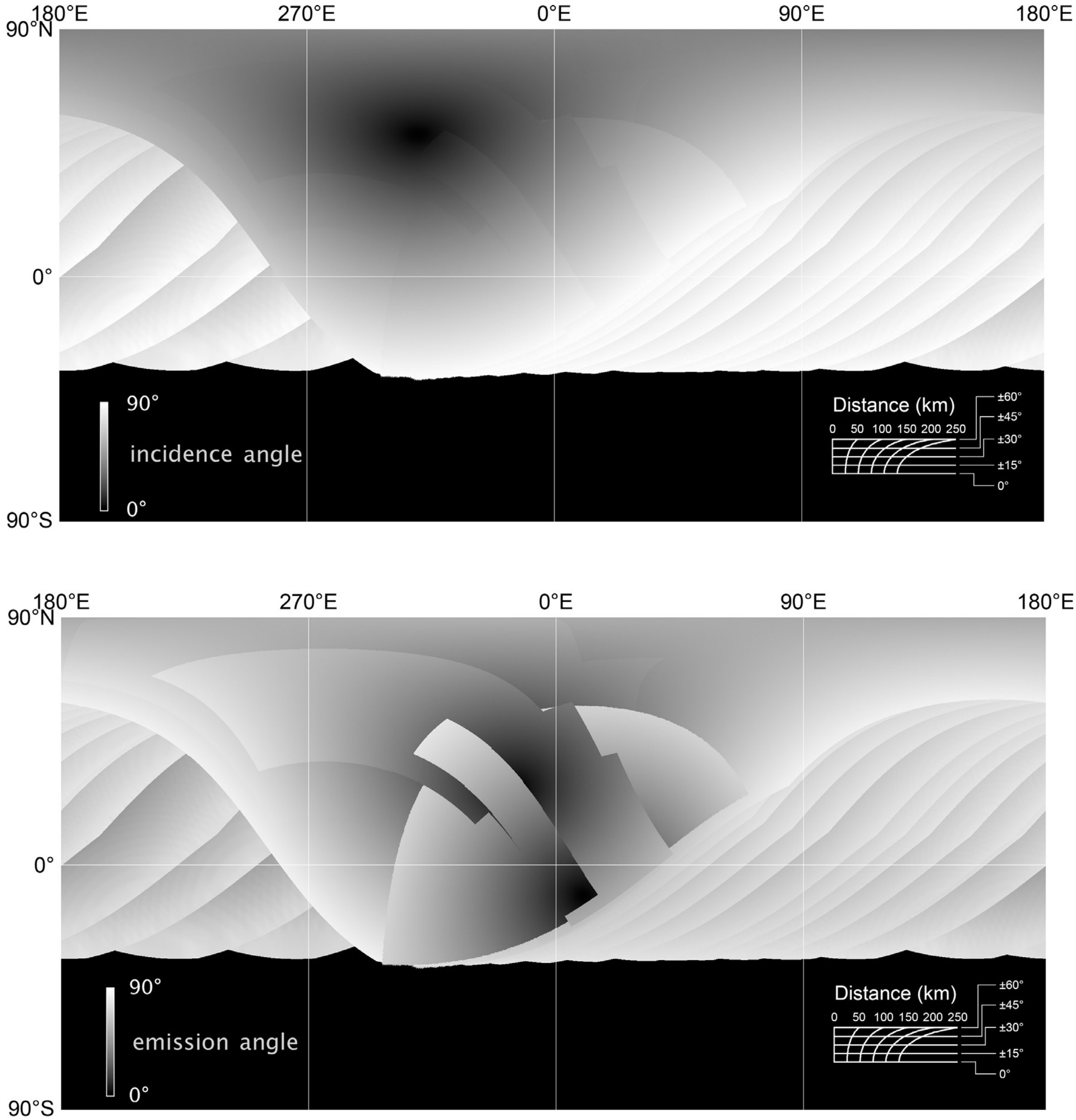

Fig. 2. (*continued*)

bundle adjustment solution, and so we implemented a “two-solution” control network strategy. For the purpose of producing a cartographically reliable base map and stereogrammetric DEMs of high geometric fidelity, we used only LORRI framing camera images in the official final global control network, as the camera distortion model in ISIS is correct and reliable (Schenk et al., 2018b). (As at Pluto, the MVIC images were controlled separately, using tie points fixed to a LORRI-only base map.) The control network solution in the jigsaw program allows for the solution of the radii of each point, relative to the center of Charon. A total of 790 tie points have been mapped to date (Fig. 5) at variable density across the surface. Most of these were on the encounter hemisphere due to the greater frequency of high-resolution imaging observations.

For all observed locations on the surface, the best images until a few hours before closest approach were obtained by the framing camera at scales of 0.8–32 km/pixel, while a combination of LORRI and MVIC images provide the best resolution of the encounter hemisphere. All LORRI images in the final 6.4 day period form the basis of the cartographic control network. No post-encounter images were useful for mapping due to the very high phase angles of > 150°. The key MVIC scans for cartographic and stereo mapping for Charon are the 1.43 km resolution 4-color scan (C_COLOR2) (using the 650-nm “red” channel for stereo, which has the best signal-to-noise), and the 625-m resolution closest approach panchromatic scan (C_MVIC_LORRI_CA), which were used together or in combination with LORRI images.

As on Pluto, the overlap of low-resolution images from one Charon rotation before closest approach (at ∼15–32 km/pixel) with high-resolution images at closest approach (at 0.15–1.43 km/pixel) makes the correlation of tie points between the low- and high-resolution data sets rather difficult. In the low-resolution approach images one Charon day earlier, tie point quality standards were necessarily lower in order to accumulate sufficient points to register the images and integrate the network around the full 360° of longitude. Definable high-contrast features are uncommon in the approach images, and craters are nearly impossible to identify, except for those with diffuse bright ray patterns. Hence we rely on bright spots and other ‘fuzzy’ albedo features. An iterative approach was employed to arrive at a satisfactory control solution, in which the validity of the control network was checked by

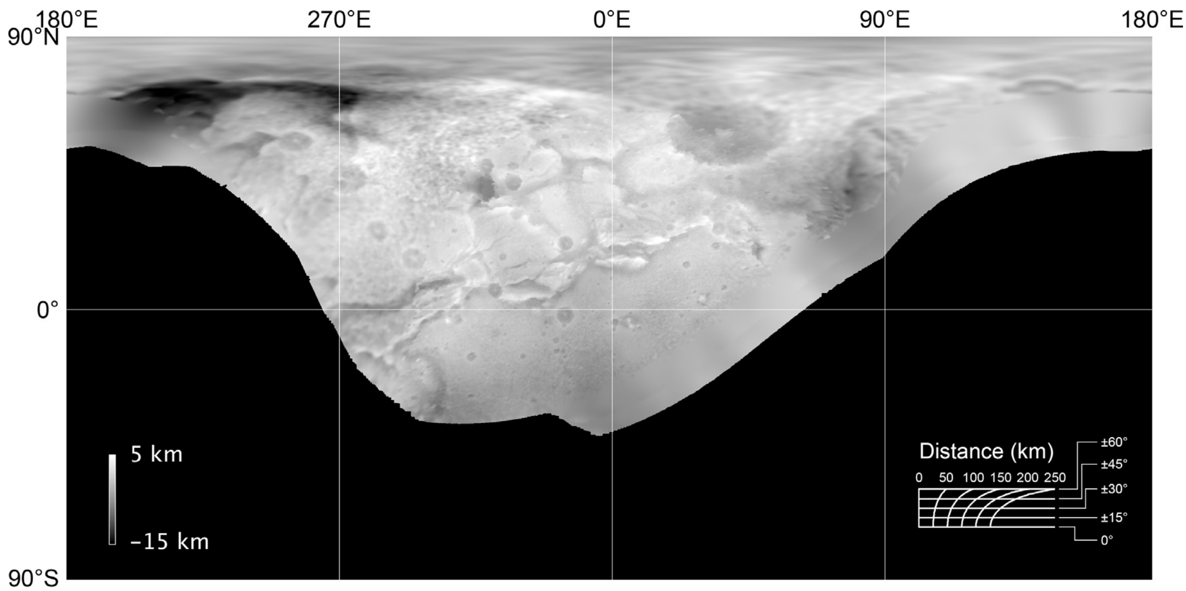

Fig. 3. Global digital elevation model (DEM) of Charon. Dark areas were illuminated or do not have resolvable stereogram metric data from the New Horizons 2015 data set. Global cylindrical map from −180° to +180°E is centered on 0° longitude.

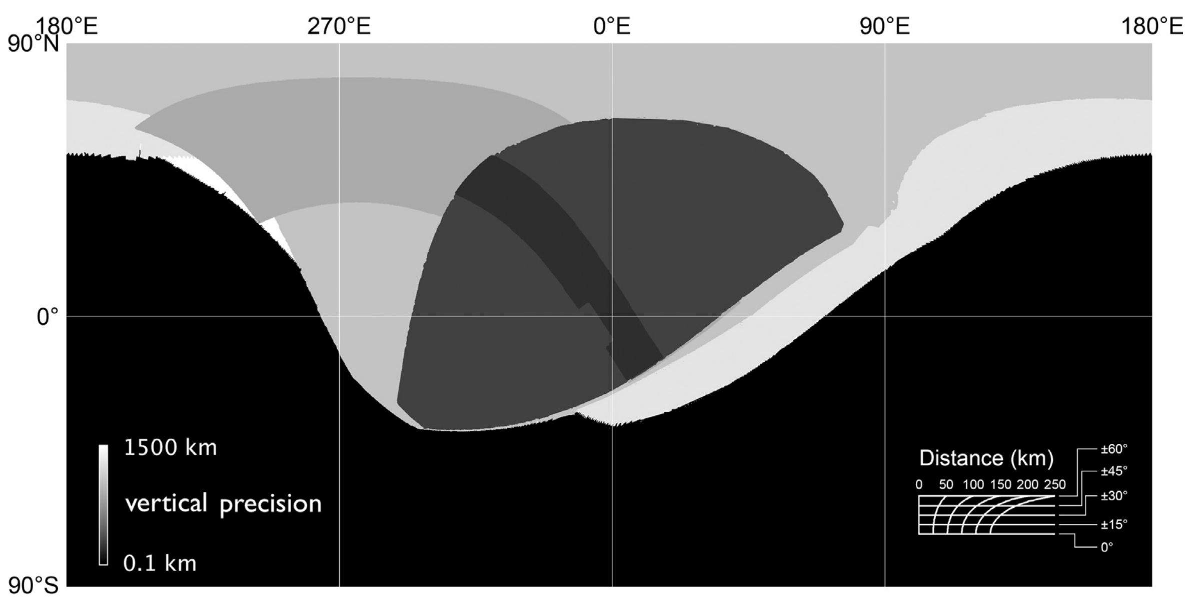

Fig. 4. Map of predicted vertical precision corresponding to Charon global topographic map in Fig. 3. Global cylindrical map from −180° to +180°E is centered on 0° longitude.

map-projection of each observation, blink comparison of overlapping maps to identify misalignment, and adjustment of tie points as needed. The resulting solution is examined and all points with high solution errors are either corrected or deleted from the network. This process is repeated until the team is satisfied that all erroneous or poorly defined points are removed and all images were aligned. The resulting updated camera vectors for the resolved Charon images form the basis of the cartographic control network, and can be obtained from the authors (PS or RB) and will be archived in the near future.

3. Topographic mapping of Charon

The most comprehensive topographic data for Pluto and Charon come from two main sources: bundle adjustments of the control network solution for the determination of radii at each point (Fig. 5; described above); and DEM production from stereogrammetric analysis of New Horizons stereo images (Fig. 3). Supplemental topographic data from limb profiles, shadow length measurements, and shape-from-shading will be addressed in a future report.

3.1. Tie point radii

As described above, tie point locations can also be solved for the radius of each point (Fig. 5), if sufficient parallax is associated with the point. The resolution of approach phase imaging is too poor to resolve highs and lows and obtain robust radii for those points. Certainly, no major topographic deviations are resolved in the approach hemisphere of Pluto, either in the tie point radii map or in shading or shadows along the terminator of the images that were acquired every ~15° of longitude.

In the high-resolution mapping areas of Charon, nearly all of the tie points contained sufficient parallax to estimate their radii. In this map (Fig. 5), the major topographic features described below are all observed, as special effort was made to accumulate a density of points

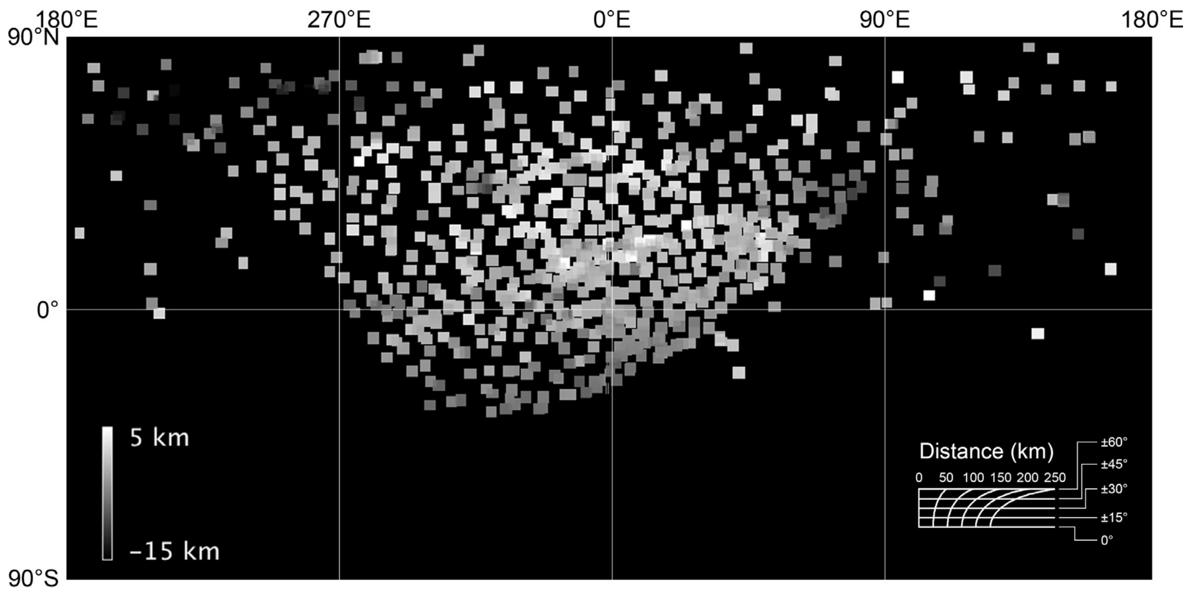

Fig. 5. Global map of tie points on Charon, shaded to show estimated radii of each point. Points have been blurred to increase their visibility. Global cylindrical map centered on 0° longitude for clarity.

Table 1
Stereo Observations of Charon.

Left Image	Right Image	Left Image Resolution (m)	Right Image Resolution (m)	DEM Vertical Precision (m)	Stereo Parallax Angle
PELR_C_LORRI	PEMV_01_C_COLOR_2	875	1425	1410	11.6
PELR_C_LEISA_LORRI_1	PELR_C_LEISA_HIRES	700	415	1140	7
PELR_C_LORRI	PELR_C_LEISA_HIRES	875	415	875	8.5
PELR_C_LEISA_LORRI_1	PELR_C_MVIC_LORRI_CA	700	150	400	53
PEMV_01_C_COLOR_2	PEMV_01_C_MVIC_LORRI_CA	1425	615	360	43
PELR_C_LEISA_HIRES	PELR_C_MVIC_LORRI_CA	415	150	100	46

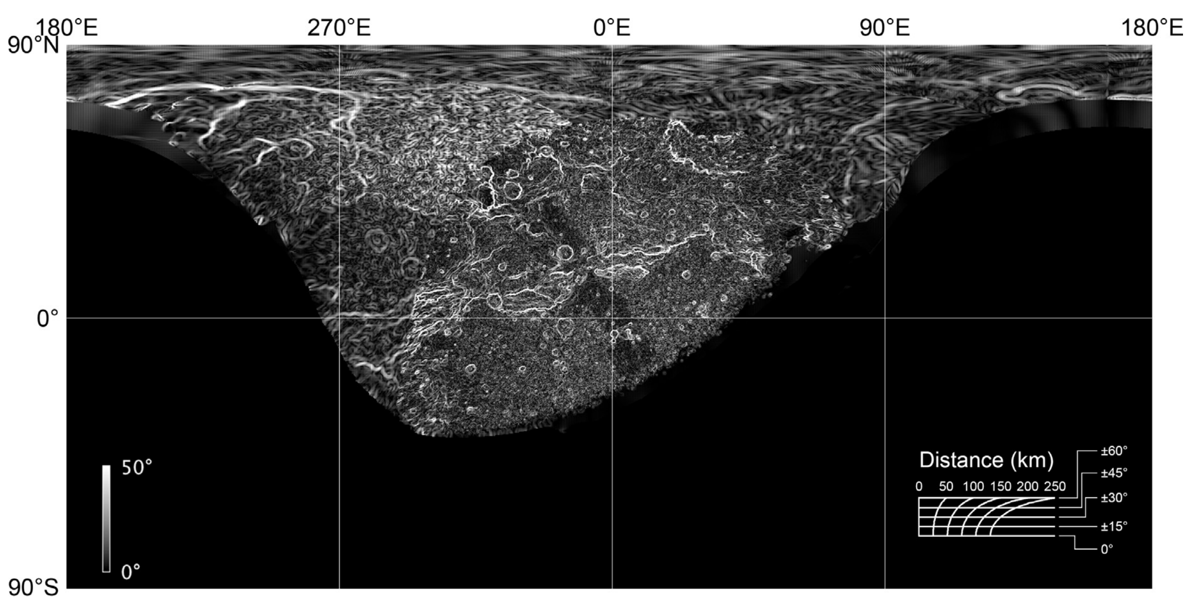

Fig. 6. Map of slopes on Charon. Global cylindrical map from −180°E to +180°E centered on 0° longitude for clarity.

across the hemisphere sufficient to resolve them. Within the limits of the tie point technique, this radii map is indistinguishable from the stereo results described below.

3.2. Stereogrammetry

Multiple useful stereo combinations are possible from the New Horizons imaging data, permitting construction of topographic DEMs (digital elevation models) of the surface capable of resolving features with nominal vertical precision of as good as ∼100 m in height in the center of the encounter hemisphere, and 400 to ∼1000 m elsewhere (Fig. 4). The precisions quoted in Table 1 for each stereo pair are estimated using the formulation of Cook et al. (1996) and are approximate. The ability of stereogrammetry software to achieve these levels

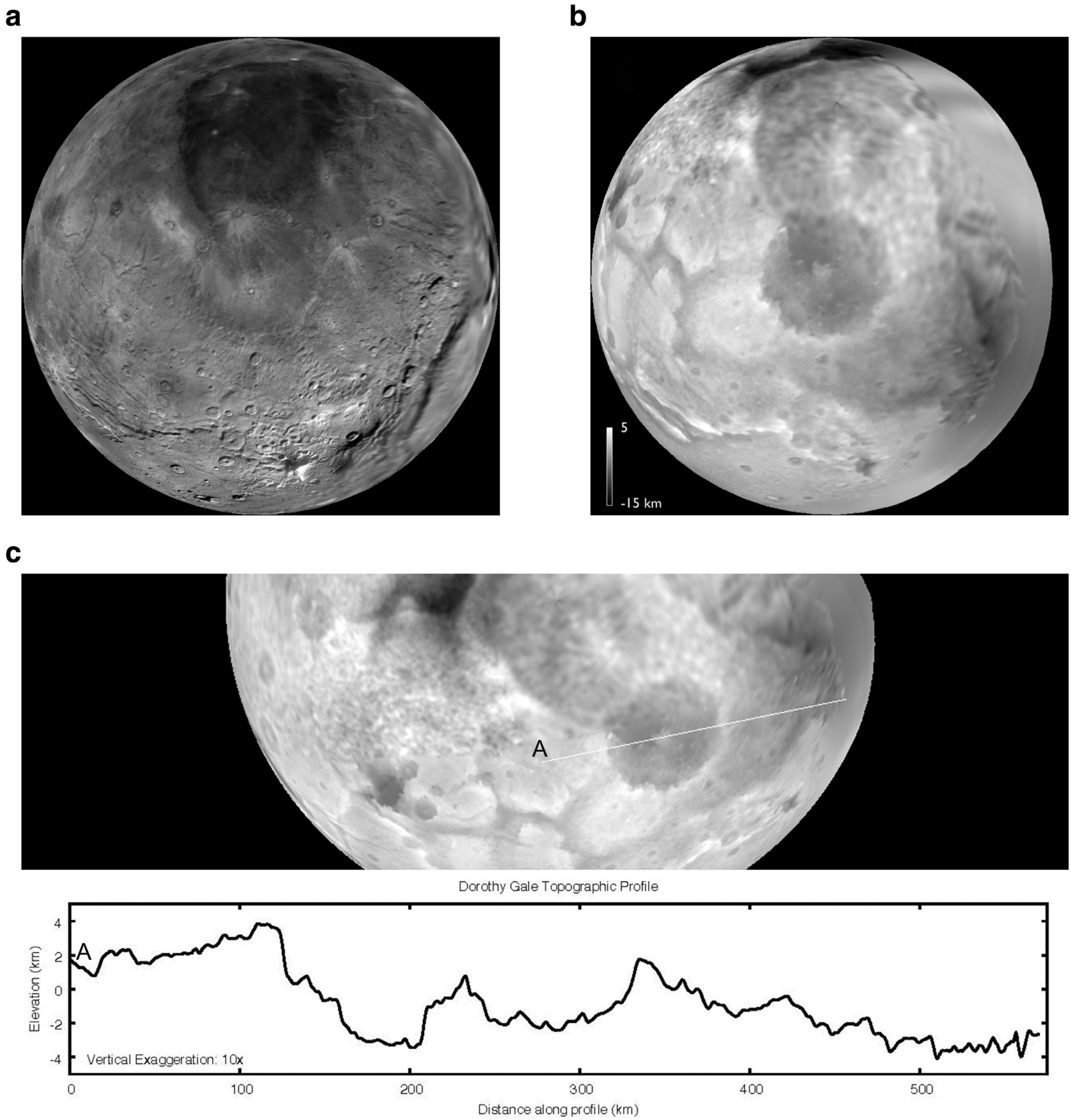

Fig. 7. Point perspective view of global image mosaic (a) and DEM elevation map (b) showing encounter hemisphere of Charon centered on Dorothy impact basin. Maps show topography and highlight many of Charon's major geologic and topographic features, including the large deep basin Dorothy. Disrupted highlands are at left, Vulcan Planitia at bottom, and deep polar troughs at top, with the dark regions of Mordor Macula at upper center. (c) Profile across Dorothy crater showing deep bowl and central peak.

of precisions has been demonstrated on other planetary bodies (e.g., Schenk and Bulmer, 1998; Schenk and Pappalardo, 2004; Schenk and McKinnon, 2009a, b). A total of 6 regional DEMs with a range of characteristic vertical precisions were constructed from the best stereo combinations (Table 1), which were then integrated into a final topographic map (Fig. 3) covering ~45% of Charon's surface.

To derive elevations over large areas using stereo imaging we use digital stereogrammetry mapping tools (e.g., Schenk and Bulmer, 1998; Schenk and Pappalardo, 2004) designed at the Lunar & Planetary Institute from ISIS code for use on Voyager, Galileo, and Cassini images of icy bodies, and used for Pluto (Schenk et al., 2018b). Like other similar stereogrammetric tools, the process involves sampling each point in the stereo image pair using areal scene recognition algorithms. Typically these use 5 × 5 pixel patches centered on each pixel in the map. The scene recognition searches for the best match to this patch in the second image and derives the parallax from the shift in position of the best match, from which elevation is computed using standard parallax equations. While distributed noise is typically inherent to scene-

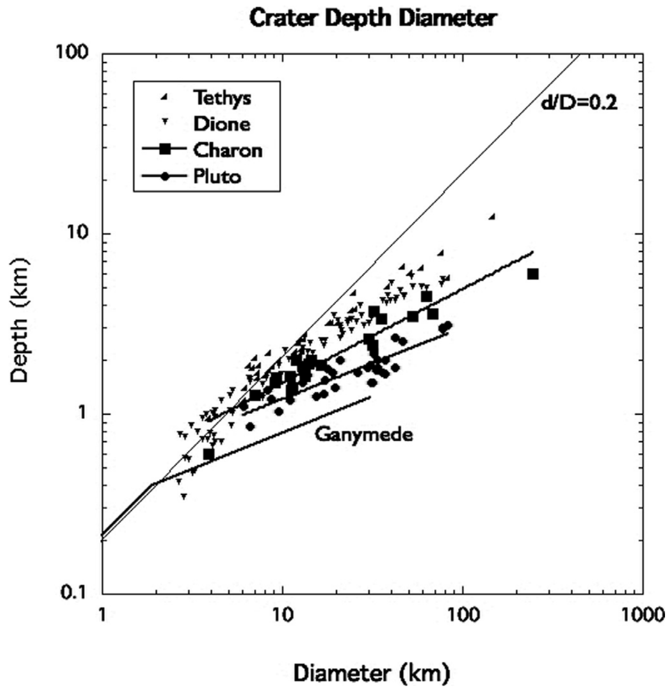

Fig. 8. Depth/diameter data for freshest complex craters on Charon (large black squares). Dark lines through data are best fit. Small circles with line are data for Pluto, showing that craters are deeper on Charon, as expected for gravity scaling of complex crater dimensions.

matching base stereogrammetry solutions, the quality of the DEM data sets for Charon is remarkably good, the noisiest areas being toward the north and west where stereo parallax and image resolution were lower and solar elevation was higher, muting morphologic details (Fig. 3). No stereogrammetric mapping was possible in the low-resolution portions of the approach hemisphere.

The quality of stereogrammetric mapping parameters and resulting integrated DEM for Charon (Fig. 4; Table 1) depending on the stereo sequences used. Due to the nested nature of the LORRI mapping coverage, horizontal and vertical precision of resulting DEMs are best along the central section of the encounter hemisphere, decreasing in quality to the east and west of the LORRI high-resolution mosaic. Best vertical precisions are as good as 100 m in the central section with post-spacing (DEM pixels) as good as < 1 km (Table 1).

DEMs of Pluto revealed wave-like 'rumpling' of the topography parallel to the scan lines in the original MVIC images (Schenk et al., 2018b). The distortions are typical of terrain models created from line-scan images obtained from a moving platform where camera-pointing vectors are required for each line. While on the order of 500 m in amplitude, these rumples tend to be subtle, and in the rugged terrains of Charon are visually difficult to detect. In contrast to Pluto, we have geometrically reliable LORRI-to-LORRI stereo over Charon's encounter hemisphere. The highest resolution MVIC-MVIC stereo combination (Table 1) is noticeably distorted with respect to the LORRI solution and this warping or "rumpling" in MVIC-based DEMs was removed before the DEMs were integrated to produce the global product (Fig. 3), as detailed in Schenk et al (2018b).

Both the global mosaic and topographic map are available now at the PDS Cartography and Imaging Sciences Node (IMG) Annex: the panchromatic global mosaic in Fig. 1 is available at https://astrogeology.usgs.gov/search/map/Charon/NewHorizons/Charon_NewHorizons_Global_Mosaic_300m_Jul2017 and the global terrain model is available at https://astrogeology.usgs.gov/search/map/Charon/NewHorizons/Charon_NewHorizons_Global_DEM_300m_Jul2017. Additionally, all of the data products described in this manuscript have been submitted for long-term archiving as part of the New Horizons PDS delivery, are currently under review, and should be available soon.

As with all digital stereogrammetric topographic mapping products, it must be remembered that the process uses a scene-matching algorithm to determine feature parallax. This degrades the resolution of the features by a factor of between 3 to 5. Smaller features on this scale may or may not be resolved in the final DEM products.

It is noted that all elevation products derived here are referenced to the estimated mean spherical radius of 606.0 km for Charon (Nimmo et al., 2017), and are not independent estimates of this mean radius.

3.3. Slopes

A map of slopes across the encounter hemisphere of Charon (Fig. 6) at effective spatial scales of approximately 1 km was derived from the integrated DEM. The quality of the slope map is sensitive to the quality of the input DEM data. The northern terrains tend to have noisier elevation data and hence a noisier slope map. Slope data reported in this text are from the higher quality central sections of the data. Small geologic features such as the fine-scale detail within Vulcan Planitia (Moore et al., 2016) are not resolved in either the DEM or the derived slope maps, but most recognizable features are.

4. Charon: topographic characteristics

Charon, similar in size to the mid-sized icy moons of Saturn and Uranus, is noticeably different in character from Pluto, both geologically (Moore et al., 2016) and topographically (Schenk et al., 2018b). Beyer et al. (2017) summarized the basic topographic characteristics of tectonic features on Charon, and here we describe in more detail the fundamental data sets and revisit the characteristics of Charon's global and regional topographic and physiographic signature based on the final global map products. As for Pluto (Schenk et al., 2018b), the control network solution by which camera kernels were updated for Charon images were also solved for the radii of each of the 790 tie points. This elevation map (Fig. 5), though sparser in density than the DEMs, is indistinguishable from the stereogrammetric solution (Fig. 3), and we regard both data sets as reliable for regional elevation determinations, within the limits of the data set as it is distributed around the sphere of Charon.

4.1. Disruption of Oz Terra highlands

As described by Moore et al. (2016), Beyer et al. (2017), and Robbins et al. (2017) the resolved portions of Charon can be divided into two fundamental geologic terrains: the fractured Oz Terra that dominates the northern hemisphere, and the rolling apparently resurfaced plains of Vulcan Planitia to the south. On top of this is overprinted the large circular low albedo region at the illuminated pole, Mordor Macula, within Oz Terra. (We note that this report uses both informal and IAU-approved names for features. The list of currently approved names can be found at the USGS Planetary Nomenclature website [https://planetarynames.wr.usgs.gov]).

Oz Terra is moderately cratered (Singer et al., 2017), with widely scattered craters large and small. The largest of these, Dorothy, is ~240 km in diameter and 6 km deep (Fig. 7). Dorothy has a central peak ~4 km high, which is broadly similar to central peaks found on Saturn's icy moons (White et al., 2013, 2017). For Charon, the inferred depth/Diameter(d/D)-based simple-complex transition diameter for unmodified craters on all terrains (Fig. 8) is ~6 km (+/−1.5 km), consistent within the uncertainty with measurements on the similar-sized icy saturnian satellites (White et al., 2013, 2017). Although the transition diameters are similar, the slope of the least-squares-fit to the complex crater d/D data is significantly shallower and the associated depths of larger craters on Charon are shallower by up to 1 km

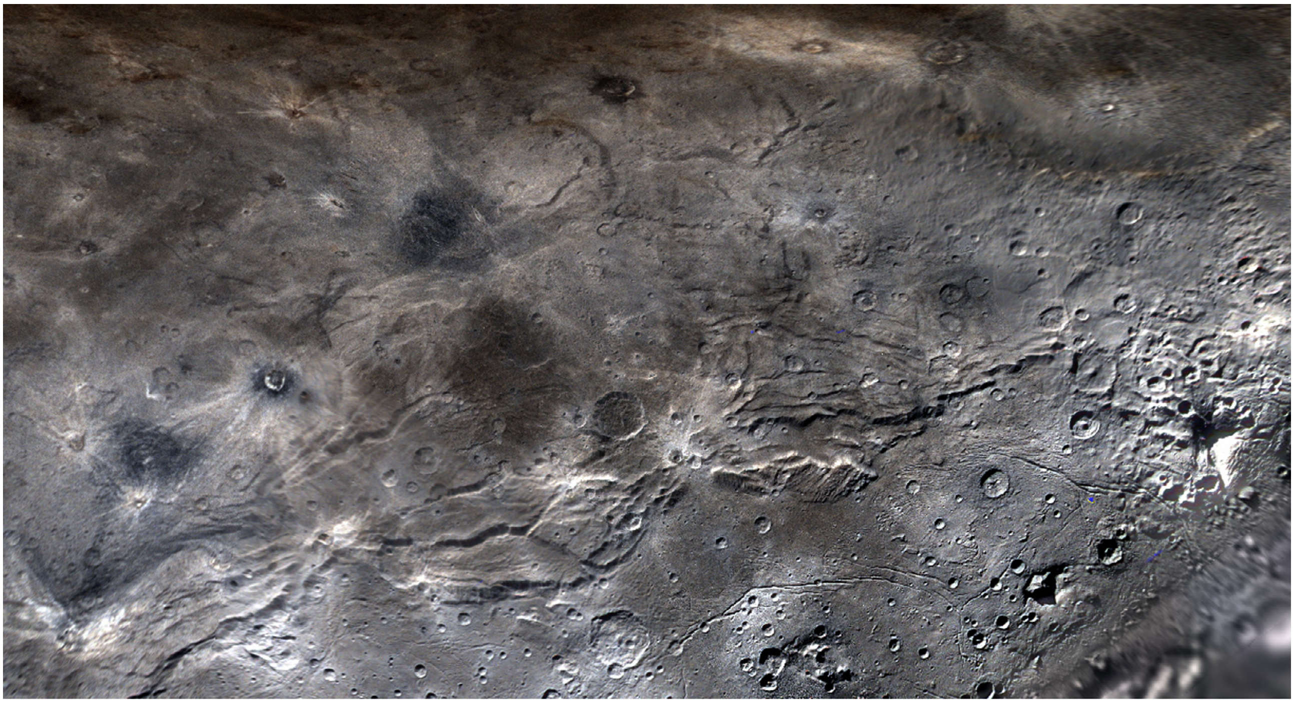

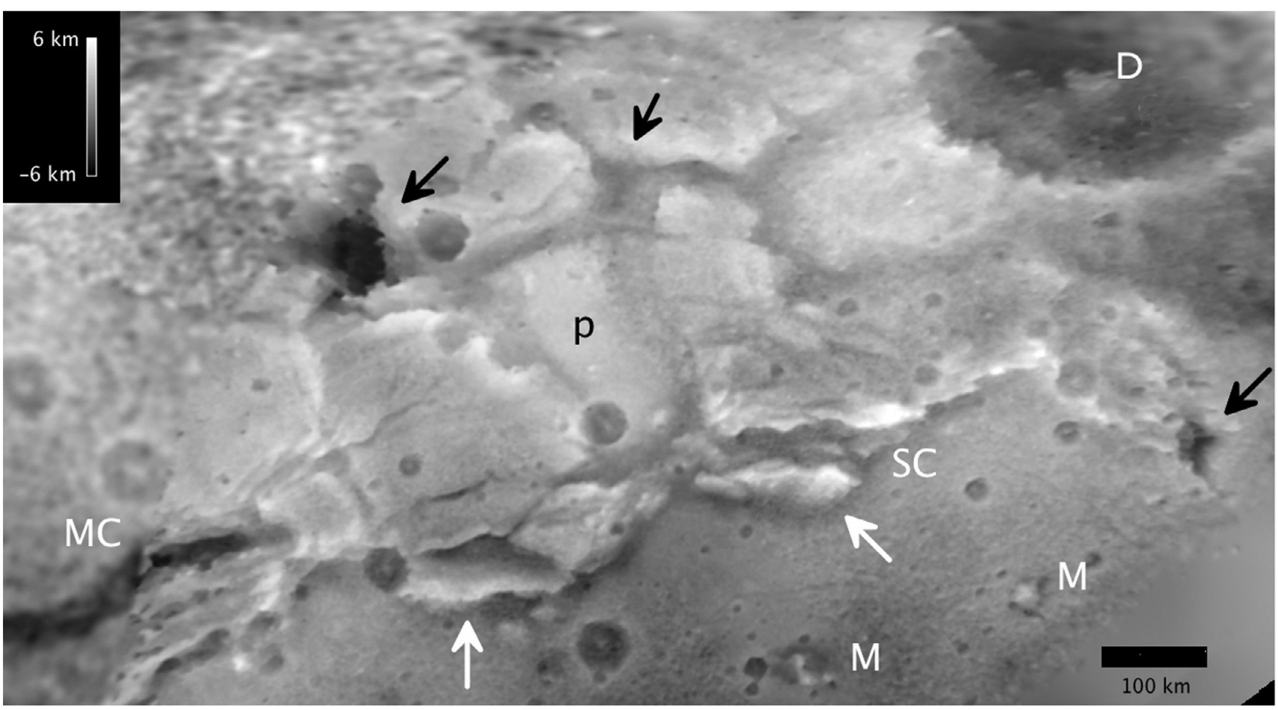

Fig. 9. (a) Disrupted terrains of Oz Terra and resurfaced plains of Vulcan Planitia, from global color mosaic (top) and DEM (bottom). Trough network evident in topography is only subtly expressed in the base map. Black arrows indicate deeper depressions at the intersections of troughs, including Matahourua Planitia at the left arrow. Smoother plains of Vulcan Planitia are across bottom of scene. White arrows indicate two prominent tilted blocks; one tilted north, the other tilted south. (p) indicates outlier of smooth plains similar those of Vulcan Planitia, (M) indicates two isolated massifs rising above the smooth plains, and surrounded by depressed asymmetric troughs or 'moats.' A detached unit of these plains occurs near center (p) and truncated fractured blocks to either side. Dorothy (D) is at upper right and two of the prominent troughs along the plains-highland board are indicated (Mandjet Chasma [MC] and Serenity Chasma [SC]). A network of mostly east-west trending linear graben is also superposed on the larger polygonal network of troughs and crustal blocks (Beyer et al., 2017). These graben-like fractures and fault scarps appear to be somewhat better preserved and to post-date terrain break-up, indicating a possible second generation of disruption. North is to the top in all views unless noted. In this view, 12 km of relief is shown. Scene is 1250 km across. The color version of the image mosaic is from the 4-color global mosaic (Fig. 1) and uses MVIC 875, 625, and 475 nanometers filter images. (b) Representative topographic profiles across Oz Terra and boundary with Vulcan Planitia to the south. Insets show profile locations in global DEM from Fig. 3. (c) Stereo pair of region shown in Fig. 9a, highlighting the troughs and titled blocks along the boundary between the disrupted plains of Oz Terra (left side) and Vulcan Planitia (right side). The bounding trough (or moat) along the outer edge of the Vulcan Planitia is also evident. Note that orientation is different to align stereo pair for viewing. Image resolutions are ~1400 and 615 km/pixel. Figure format allows user to view in either wall-eyed mode (left-center) or cross-eyed mode (center-right). Red-blue anaglyph version of this figure is available in Supplementary Fig. 1. (For interpretation of the references to colour in this figure legend, the reader is referred to the web version of this article.)

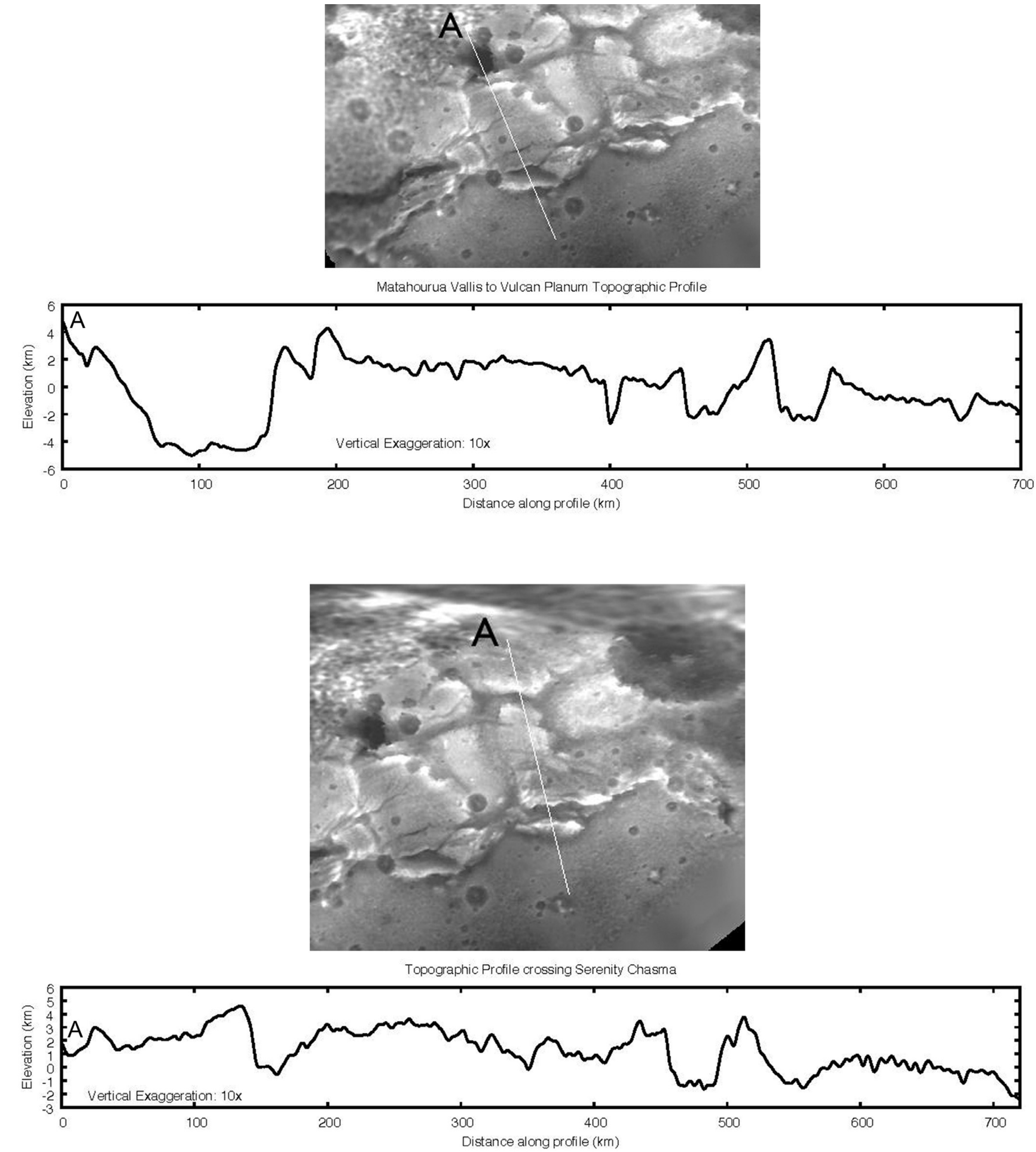

Fig. 9. (*continued*)

compared to those on Saturn's icy moons, despite the similar surface gravity and icy compositions (Fig. 8). These differences may indicate that complex crater formation on Charon may initiate under similar conditions but that the collapse process is more complex or complete on Charon. Alternatively, the expected lower impact velocity at Charon compared to the saturnian satellites could result in effects not captured by the simple gravity scaling (Bray and Schenk 2015).

The terrains of Oz Terra (Fig. 9) are broken into large polygonal crustal blocks ranging from 60 to 250 km across by a network of broad troughs several kilometers deep (Moore et al., 2017; Beyer et al., 2017; Robbins et al., in prep). An irregular depression ~4.5 km deep (Matahourua Planitia, Fig. 9) is located at the intersection of some of these linear troughs. The southern margins of Oz Terra are defined by deep troughs and scarps and fault-bounded blocks a few hundred kilometers long and oriented mostly parallel to the terrain boundary (Moore et al., 2016; Beyer et al., 2017). The surfaces of several bordering blocks are noticeably tilted, one southward, the other northward (Fig. 9), with mean surface tilts of 5–6°, and heights from low-to-high points of

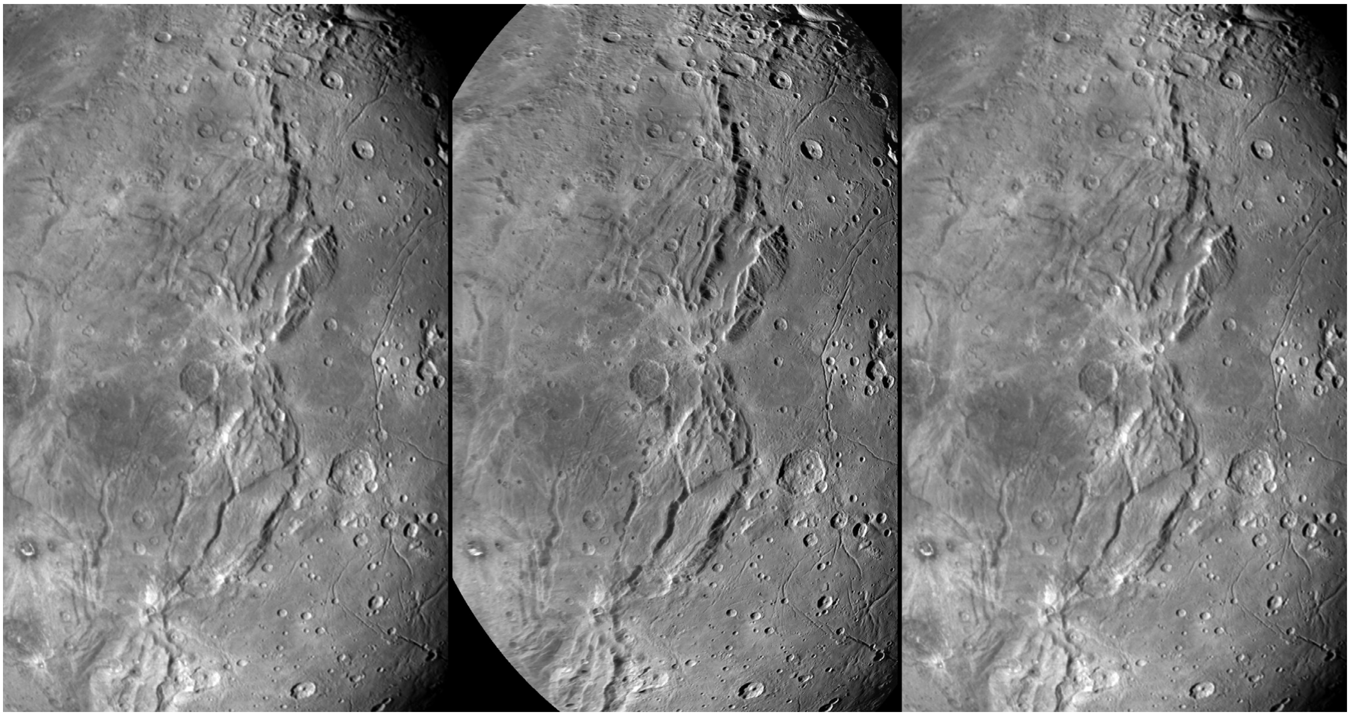

Fig. 9. (*continued*)

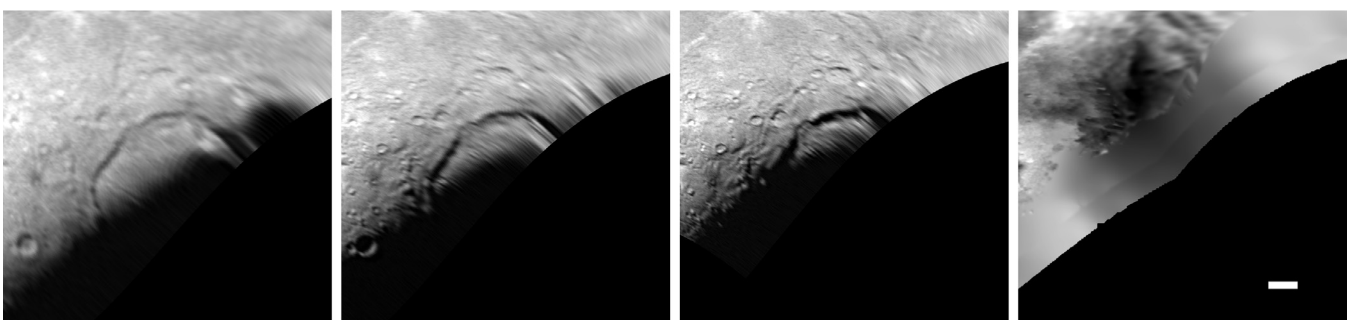

Fig. 10. From left-to-right: three views of Argo Chasma region under increasingly lower solar illumination, and current DEM of region (right). Changing view highlights double-walled trough that forms this feature, which could be a moat similar to that seen in Fig. 9 along the outer margin of Vulcan Planitia. The DEM (right) shows that Argo Chasma and the surrounding area are depressed relative to terrains to the west and north. Area enclosed by Argo Chasma corresponds to the circular unit in the center of the right half of Fig. 1. Cylindrical map projection centered at 15°, 90°E. Image resolutions range from ~3.7 to 1.5 km/pixel. Scene is ~600 km across; scale bar is 100 km.

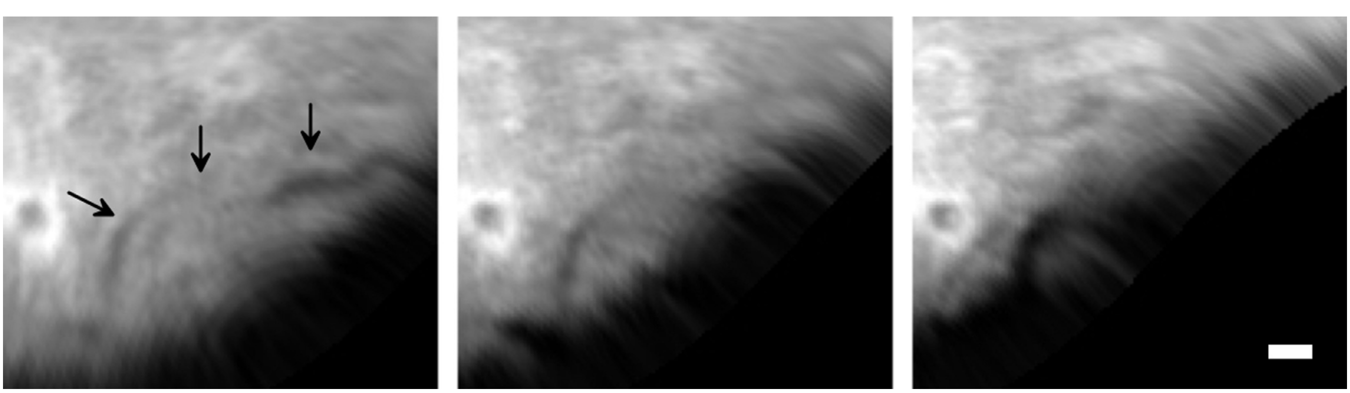

Fig. 11. From left-to-right: 3 views of curvilinear dark feature in low-resolution approach hemisphere images, under increasingly lower solar illumination illustrating apparent south-facing topographic scarps, perhaps related to those on the northern margins of Vulcan Planitia (e.g., Fig. 9). View is centered on 10°, 152°E and is ~1100 km across. Note apparent bright ray crater ~90 km across at far left center. Scene is ~600 km across; scale bar 100 km.

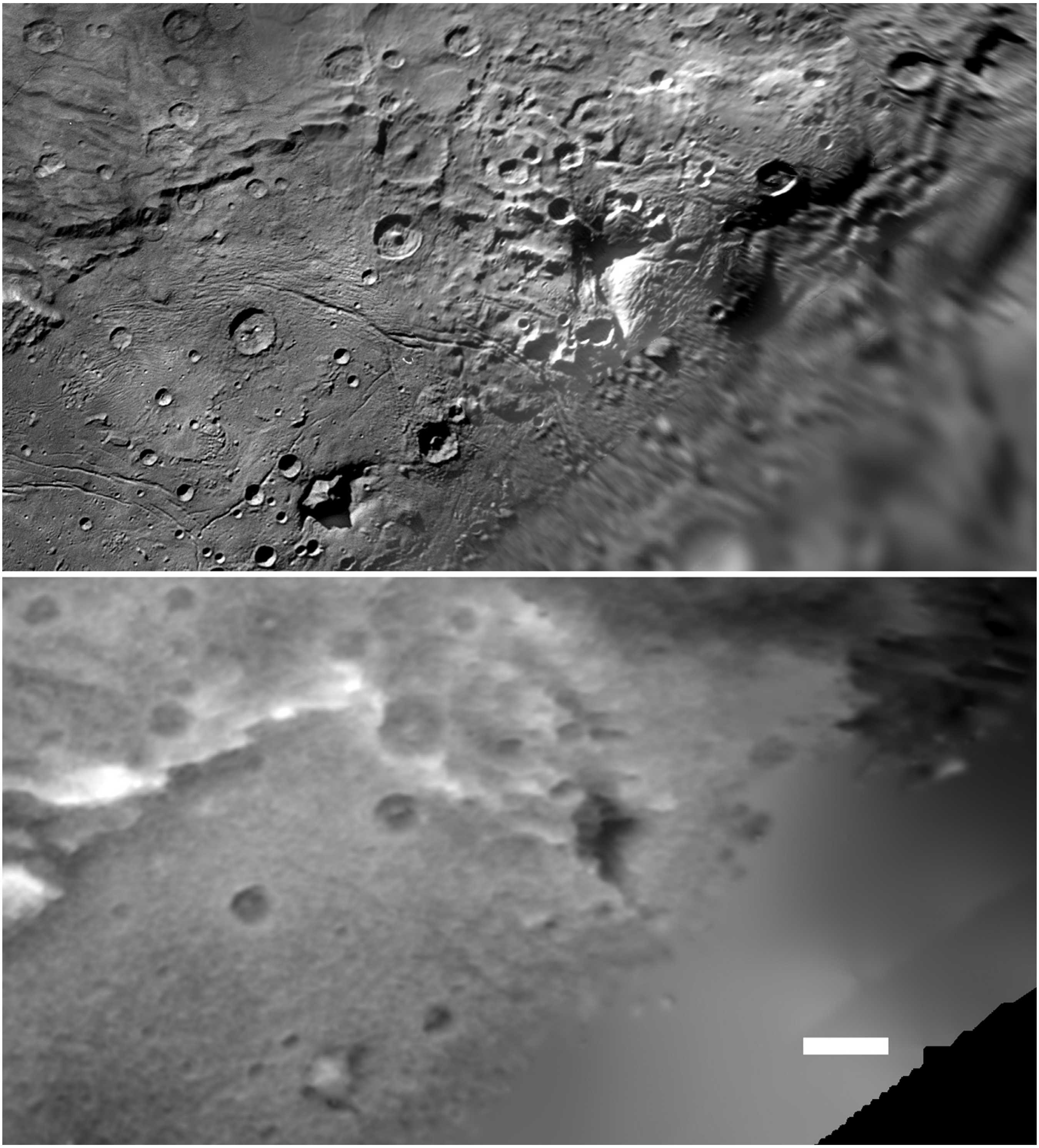

Fig. 12. Eastern exposure of Vulcan Planitia, from global color mosaic (top) and DEM (bottom). Scene highlights complex rugged terrains associated with deep depression in center. Kubrick Mons is the solitary peak at center bottom. The small depression at center is ~4.5 km deep. Note also the shadowing at center right indicating scarps and topography. Blurry areas are derived from lower resolution approach stereo images. Scene is 660 km across; north is up; scale bar is 50 km. Topographic range shown is −6 to +6 km.

4.5–5.5 km. The highest of these block crests rises ~6 km above mean Charon radius and are likely the highest standing features on the mapped portion of the surface. The large polygonal blocks at higher latitudes have undulating surfaces but are not appreciably tilted in the way the border blocks are. The steepest non-crater surfaces on Charon occur along the scarps of these tilted blocks along the boundary between the two terrains (Fig. 7), which have slopes of 40–50°.

Like Pluto, the non-encounter or approach hemisphere of Charon was observed from greater distances with pixel scales from 30 to 2 km/pixel. Little reliable stereogrammetric data can be extracted within this area, except in the north where the encounter data extend 20–25° beyond the pole itself. Some low-resolution topographic data can be obtained immediately to the east of the encounter hemisphere using approach images. The base map reveals a quasi-circular patch of terrain

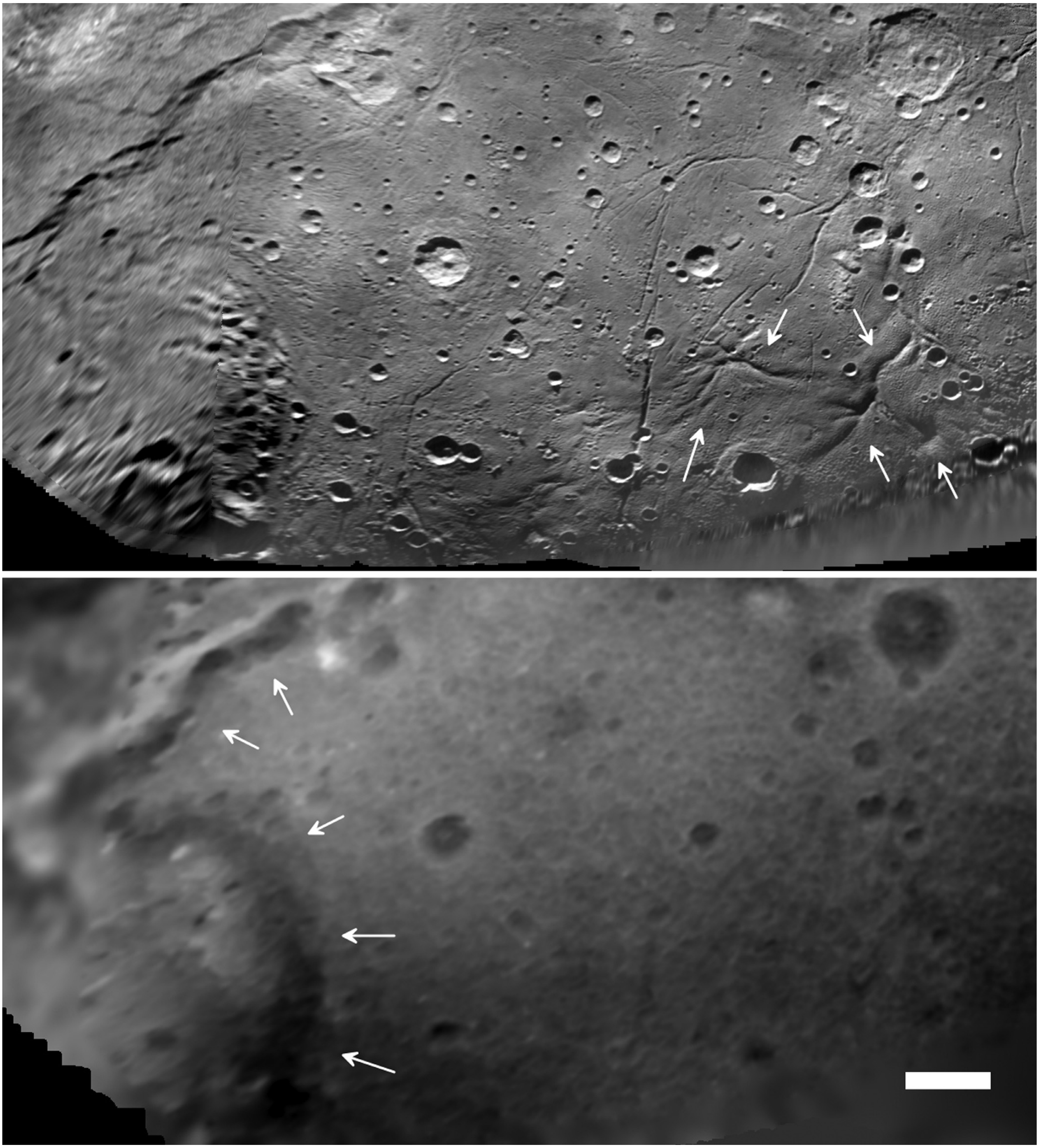

Fig. 13. Western exposure of Vulcan Planitia, from global color mosaic (top) and DEM (bottom). Scene highlights depressed trough or 'moat' along border of Vulcan Planitia (arrows in DEM, bottom) with highlands and rugged massifs to both the north and west. Arrows in image mosaic (top) denote area of converging sinuous troughs, which are associated with some of the lowest portions of Vulcan Planitia. Scene is 750 km across; north is up; scale bar is 50 km. Topographic range shown is −6 to +6 km.

almost 400 km across in this area and centered at 15°, 90°E (Figs. 1, 10). This patch appears to be smoother at kilometer scales compared to surrounding terrains and is roughly bounded by a arcuate scarp or double-walled trough informally named Argo Chasma (Moore et al., 2016; Beyer et al., 2017; Robbins et al., in prep). The height of the northern flank relative to the southern flank is difficult to assess (Fig. 10), but the textural difference suggests that the circular patch interior to the outer scarp of Argo Chasma may be an outlier or eastward extension of the Vulcan Planitia resurfaced deposits. If true, Argo Chasma would be an example of a bounding 'moat' of the type seen along the edge of Vulcan Planitia in the high-resolution mapping area (next section).

The relatively smooth unit and associated Argo Chasma structure (Fig. 10) lie within a broader depression ∼550 km across centered in the same region and along the eastern margins of the integrated global DEM (Fig. 3) but considerably larger than the arcuate Argo Chasma itself. Though low in resolution, the large irregular depression is confirmed by the tie-point radii map (Fig. 5). Although more poorly resolved than other terrains to the west, it is evident that this enigmatic depression is not a simple bowl but has some poorly resolved structural elements. Despite this, the outer regions of the depression are not defined by any discrete scarp or ridge and its origin is not known.

Low-resolution approach images reveal additional curvilinear dark features immediately to the east of Argo Chasma (Fig. 11) near the 180° meridian. Although no topographic data are available here, shadowing suggests that these may be additional examples of bounding scarps or moats similar to those seen along the southern margin of Oz Terra (Fig. 9; Beyer et al., 2017).

4.2. Topography of Vulcan Planitia

Vulcan Planitia forms broad contiguous undulating plains south of Oz Terra (Moore et al., 2018). These plains extend into the dark zone of Charon and its southern extent is unknown but the northern margin is well observed. Although scarred by pitting and curvilinear ridges, troughs and fractures, Vulcan Planitia is relatively contiguous and devoid of major tectonic disruptions, at least compared to the terrains of Oz Terra (Beyer et al., 2018; Robbins et al., in prep). A nearly contiguous “moat” or trough occurs along the outer margin of Vulcan Planitia (Figs. 3, 9, 12; Moore et al., 2016), with the side along the northern terrains being higher in elevation by a kilometer or so. This bounding trough forms convex outward-facing scarps 1–3 km high along the outer edge of the plains. Similar moats surround the isolated mountains that rise 3–6 km high in scattered locations of eastern Vulcan Planitia (Fig. 12). This marginal relief suggests that the materials that resurfaced the plains were relatively viscous and resisted outward flow, forming a marginal rampart (Moore et al., 2016; Beyer et al., 2018). Liquid or liquid-solid ammonia/water mixtures (and other water mixtures) typically have higher viscosities than water alone (e.g., Kargel et al., 1991; Durham et al., 2010) and could satisfy these constraints (see discussion in Beyer et al., 2018).

Numerous topographic features occur within Vulcan Planitia. A 55-km wide and 6-km-deep irregular pit occurs in the eastern portion of Vulcan Planitia (Fig. 12). The prominent mountains informally known as Clarke Mons and Kubrick Mons (Fig. 9) that rise abruptly from the Vulcan Planitia plains (Moore et al., 2016) stand 2.5–3 km above the local plains but 3.7–4 km above the depressed moats that surround them (Figs. 9 and 12). Another mountain, Butler Mons, was observed at lower resolution at −11°, 39°E (Fig. 1). Shadows indicate a height of at least 4.5 km. Mountains are observed east of 0° longitude but not to the west, at least within the illuminated areas. One large area west of 0° longitude features large curvilinear grooves, some of which converge in twisted intersections (Fig. 13).

Aside from widely dispersed arcuate troughs or rilles (Fig. 13), most areas of Vulcan Planitia are relatively smooth at 400–600 m pixels scales. At < 200 m scales the surface of Vulcan Planitia is often scarred by kilometer-scale pits and additional narrow curvilinear troughs or grooves (Moore et al., 2016). These smaller features are not resolved in the stereo DEMs and are the subject of ongoing topographic mapping using the highest resolution mapping data sets.

A key constraint in assessing origins of Vulcan Planitia is the mean elevation of the plains with respect to the apparently older unresurfaced Oz Terra terrains to the north. Of course, any measure of the effective altitudes of any rugged or undulating terrain depends on how it is sampled; e.g., whether the greatest deviations are included in the samples or avoided as outliers. Sampling all well resolved DEM data of each terrain (Table 2) we derive mean elevations of ∼0.1 km (standard deviation of 2.7 km) for Oz Terra and of −1.15 km (standard deviation of 1.7 km) below the mean Charon radius for the observed portions of Vulcan Planitia. Sampling the northern disrupted terrain of Oz Terra excluding the 12-km-deep polar trough and basin described below (Fig. 9) gives a mean elevation of ∼1.1 km above mean radius (standard deviation of 1.7 km), which now indicates that Vulcan Planitia is likely 1–2 km lower on average in elevation than northern terrains (and motivating the change from “Vulcan Planum” in earlier literature). This is observed in both the radii map (Fig. 5) and stereogrammetric DEM (Fig. 3), and indicates that this topographic trend is robust within the constraints of the available data which cover only ∼45% of the surface. We explore the topographic properties of these terrains in more detail in the Discussion section.

Table 2
Topographic Characteristics of Charon and Major Geologic Terrains.

Terrain	Area	Mean	Std. Dev.	Variance	Skew	Median	Mode
Charon (all)	1.76	−0.19	2.53	6.43	−0.45	0.19	1.49
Oz Terra	1.25	0.13	2.65	7.01	−0.70	0.75	1.49
Vulcan Planitia	0.43	−1.14	1.70	2.90	−0.16	−1.05	−1.36

*All units in 10^6 km^2 (area) or km.

An important consideration is whether the division of Charon in the DEM region into northern disrupted terrains and southern resurfaced terrains has biased the topographic solution in either direction. The mean elevations of the large blocks that make up the northern terrains are relatively consistent, as measured across the tops of the polygonal blocks. If we assume that these blocks represent an effective equipotential surface for the older original crust in areas resolved and unresolved, then this consistency across the northern tier suggests that the global shape model shown in Fig. 3 and the inference that Vulcan Planitia is depressed 1–2 km is realistic.

4.3. Topography of Charon's North Polar region

The other dominant feature on Charon is its north polar dark “cap” (Stern et al., 2015; Grundy et al., 2016b), also known informally as Mordor Macula. The darker core of this albedo feature is ∼375 km across, although a broader less dark halo surrounds it (Fig. 14). The topographic signature associated with Mordor Macula is complex (Fig. 14), indicating that the dark materials are sometimes locally influenced by topography.

Referencing radially from the geographic pole, the quadrant of Mordor Macula centered on 90°E longitude is roughly the same elevation as the broken highlands elsewhere across the northern hemisphere, and topography is poorly correlated with albedo. In the opposing 270°E quadrant, relief across Mordor Macula slopes gently downward away from the pole to a relative elevation of approximately −2 km below the mean. These values are within the variability observed elsewhere within the northern hemisphere and are not unusual. In the 270° quadrant, a curvilinear ridge 1–2 km high extending from 210° to ∼360°E and between 72° and 77° latitude forms the outer edge of the dark core of Mordor Macula (Figs. 14 and 15). The ridge appears to act as a partial lateral barrier to dark material emplacement, with some of the darkest deposits occurring on the pole-facing slopes but little or no albedo or color signature on the equator-facing slopes. This relationship would be consistent with topographic impedance of materials moving laterally from the polar region, or more likely local thermal environments controlled by slope direction. The greatest negative relief on Charon occurs just outside this ridge along the outer margin of Mordor Macula. This is the elongate distorted-Y shaped trough and basin Caleuche Chasma, centered along latitude 70° between 200° and 280°E, which reaches a maximum depth of approximately 13 km below mean radius (Figs. 14 and 15), the deepest features known on Charon. The darkest deposits do not cross over the ridge into these deep features, however.

The dark materials associated with Mordor Macula are also absent or less concentrated on the floors of two large craters within it; 250-km-

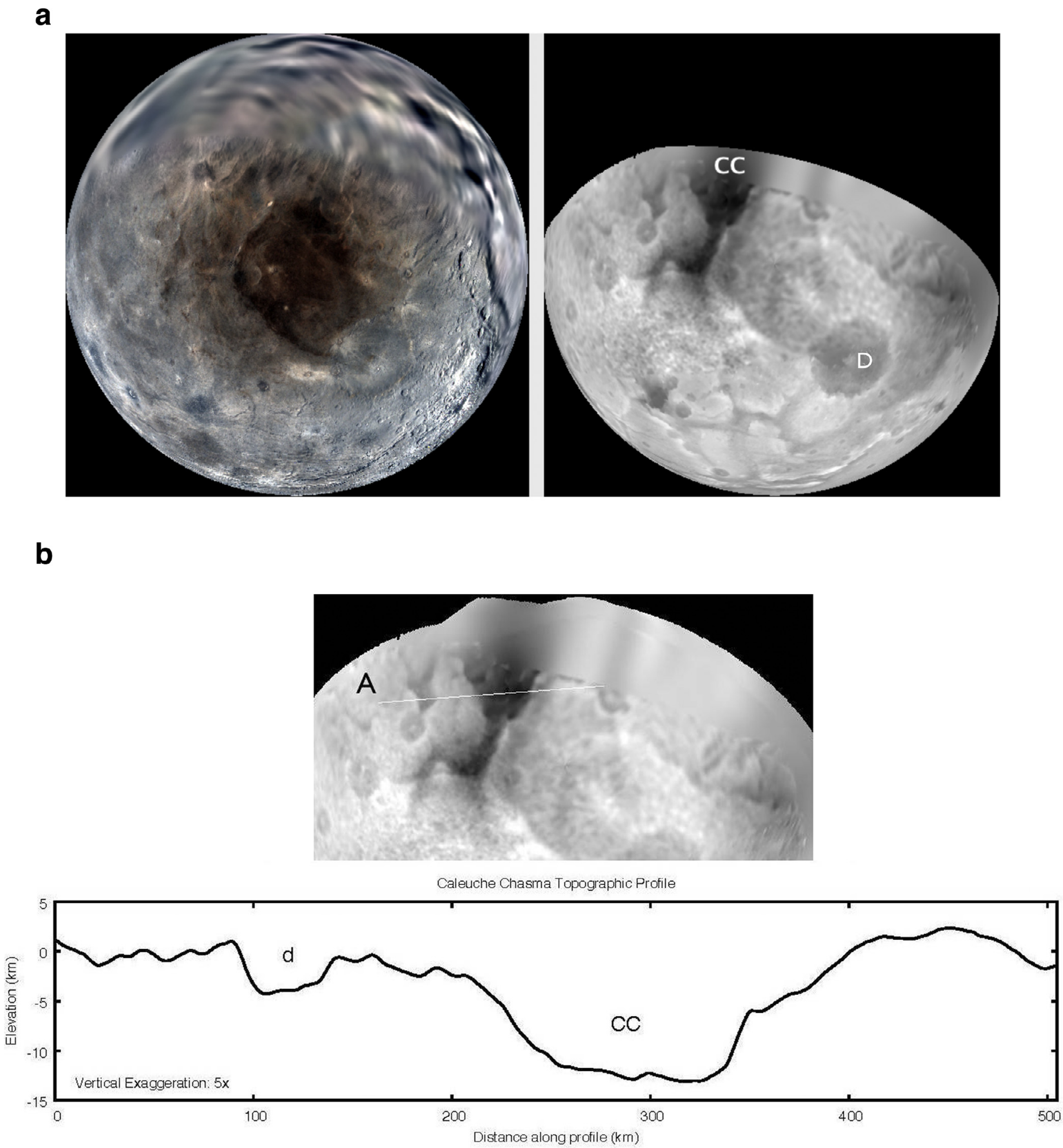

Fig. 14. (a) Section of global color mosaic (left) and DEM (right) showing orthographic view of Charon's northern hemisphere centered on the north pole and the dark region Mordor Macula. Crater Dorothy (D) and deep trough Caleuche Chasma (CC) are highlighted. Note the lack of dark reddish material in the floor of Dorothy. Topographic range shown is −14 to +6 km. The color version of the image mosaic is from the 4-color global mosaic (Fig. 1) and uses MVIC 875, 625, and 475 nanometers filter images. (b) Profile across Caleuche Chasma (CC) and small depression (d) immediately to the south. Inset shows location in map in Fig. 14a. (For interpretation of the references to color in this figure legend, the reader is referred to the web version of this article.).

wide Dorothy crater at 57°, 39°E, and an 80-km-wide crater at 72°, 144°E (Fig. 16). Both craters are several kilometers deep and form breaks in the otherwise circular pattern of Mordor Macula. Like the arcuate ridge described above, the rims of both craters appear to act as a barrier to the darkest material. Other areas near 80°, 280° are just as deep but are covered in very dark material, suggesting that elevation is a significant but inconsistent control on dark material formation. In these two craters, material properties related to impact formation peculiar to crater floors might be involved in inhibiting dark deposit formation on these two craters, rather than topography. In any case, the inconsistent albedo-topography signature across Mordor Macula and the preservation of smaller geologic features indicate that the dark deposits are likely not a discrete physical deposit with significant thickness, such as lava flows, but rather thin deposits or alteration of

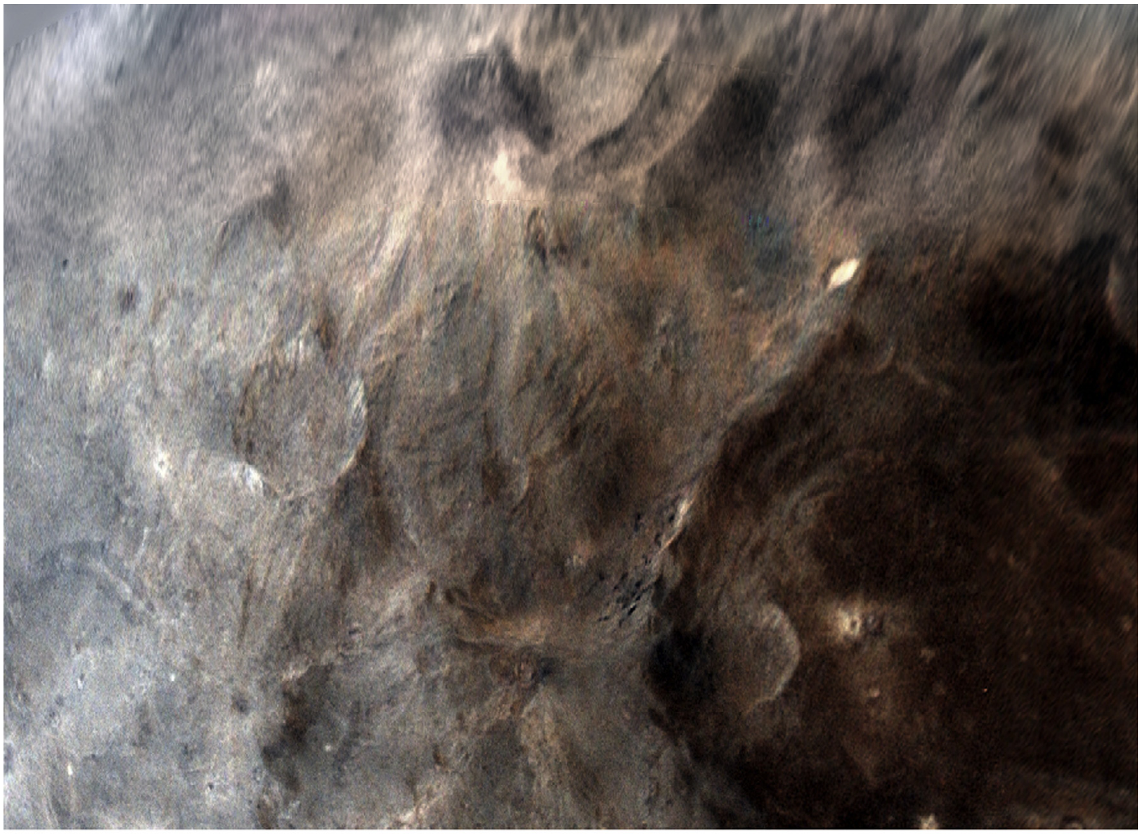

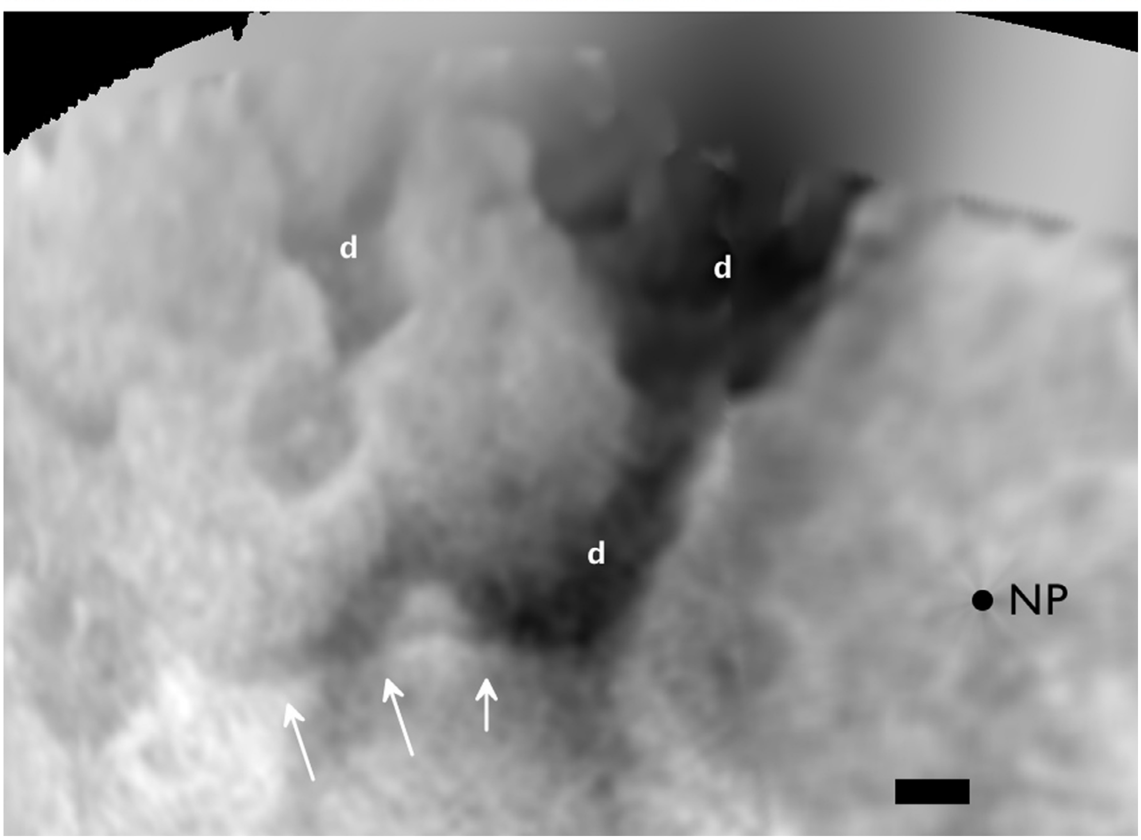

(caption on next page)

Fig. 15. (a) Section of global color mosaic (left) and DEM (right) showing fault scarps and deep chasma within Oz Terra near the +90° pole. Arrows indicate probable normal fault cutting across undulating cratered plains. Several prominent enclosed depressions (d) occur here, including the 10–16 km deep Caleuche Chasma at center. Note small dark spots at bottom center. Scene is ~450 km across; NP is north pole; scale bar is 50 km. Topographic range shown is −14 to +6 km. The color version of the image mosaic is from the 4-color global mosaic (Fig. 1) and uses MVIC 875, 625, and 475 nanometers filter images. (b) Stereo pair of region shown in Fig. 15a, highlighting the deep troughs and depressions, including Caleuche Chasma, near the north pole, and just below the large dark feature Mordor Macula. Note that orientation is different to align stereo pair for viewing. Image resolutions are ~1400 and 875 km/pixel. Figure format allows user to view in either wall-eyed mode (left-center) or cross-eyed mode (center-right). Red-blue anaglyph version of this figure is available in Supplementary Fig. 2. (For interpretation of the references to colour in this figure legend, the reader is referred to the web version of this article.)

the existing surface (e.g., Grundy et al., 2016b) partly controlled by topography and/or surface properties, requiring further study.

5. Discussion and summary

5.1. Global topographic characteristics of Charon

New Horizons has produced a remarkable series of observations of Pluto's large moon Charon, from which integrated global maps of the illuminated surface in 4 colors (including near-IR; Fig. 1) and partial global maps of topography (Fig. 3) have been produced. The topographic variability of Charon reveals a geologically complex world (e.g., Moore et al., 2016) and places invaluable constraints of geologic and geophysical processes. The topographic hypsogram of the (partial) global DEM of Charon (Fig. 17; Table 2) is significantly higher in total amplitude and different in character than that of larger Pluto (Schenk et al., 2018b). While there are no major secondary peaks in the Charon histogram like that for Sputnik Planitia at −2 km, the lower section of Charon's hypsogram has a pronounced bulge between −5 and −1 km elevation. This skew towards negative values represents a combination of various negative relief features (Fig. 17), including the depression surrounding Argo Chasma (Fig. 10), similarly deep but smaller depressions across the disrupted northern hemisphere of Oz Terra (Fig. 8), and the undulating low plains of Vulcan Planitia (Fig. 3).

The hypsogram of the disrupted terrains of Oz Terra is also skewed (Fig. 17), with a mean elevation of ~0.1 as described in the Vulcan Planitia section above, but with an offset main peak (or mode) at ~1.49 km (Table 2). The strong offset peak is related to the higher elevations of the large broken plateaus or blocks comprising much of Oz Terra (e.g., Fig. 9), with the mean elevation reflecting the contribution from the lower topography of the bounding troughs between the blocks and other depressed topography (Fig. 17). The mean elevations of the top surfaces of individual large blocks range between 1.0 and 2.5 km, indicating that the blocks started with variable elevations or thicknesses, had some degree of vertical mobility, or are responding to local stresses differently. The long tails of both the global and Oz Terra hypsograms below −5 km (Fig. 17) are due to the deep polar trough and basin of Caleuche Chasma (Figs. 14, 15) and the other deep depression, Matahourua Planitia (Fig. 9).

The topographic signature of Vulcan Planitia is unusually complex (Fig. 17), reflecting the variable elevation across its surface (roughly +1.5 to −4.5 km). The bounding moats 10–30 km wide and 1–3 km deep and isolated massifs 1–4 km high within the boundaries of Vulcan Planitia contribute but only in a minor sense. Vulcan Planitia as a contiguous unit lies at a mean elevation of −1.14 km below Charon mean and ~1.0 km below the average elevation of Oz Terra. The southern observed portions of Vulcan Planitia are the lowest in elevation, ~3.5–4.5 km below Charon mean radius. The peak (or modal)

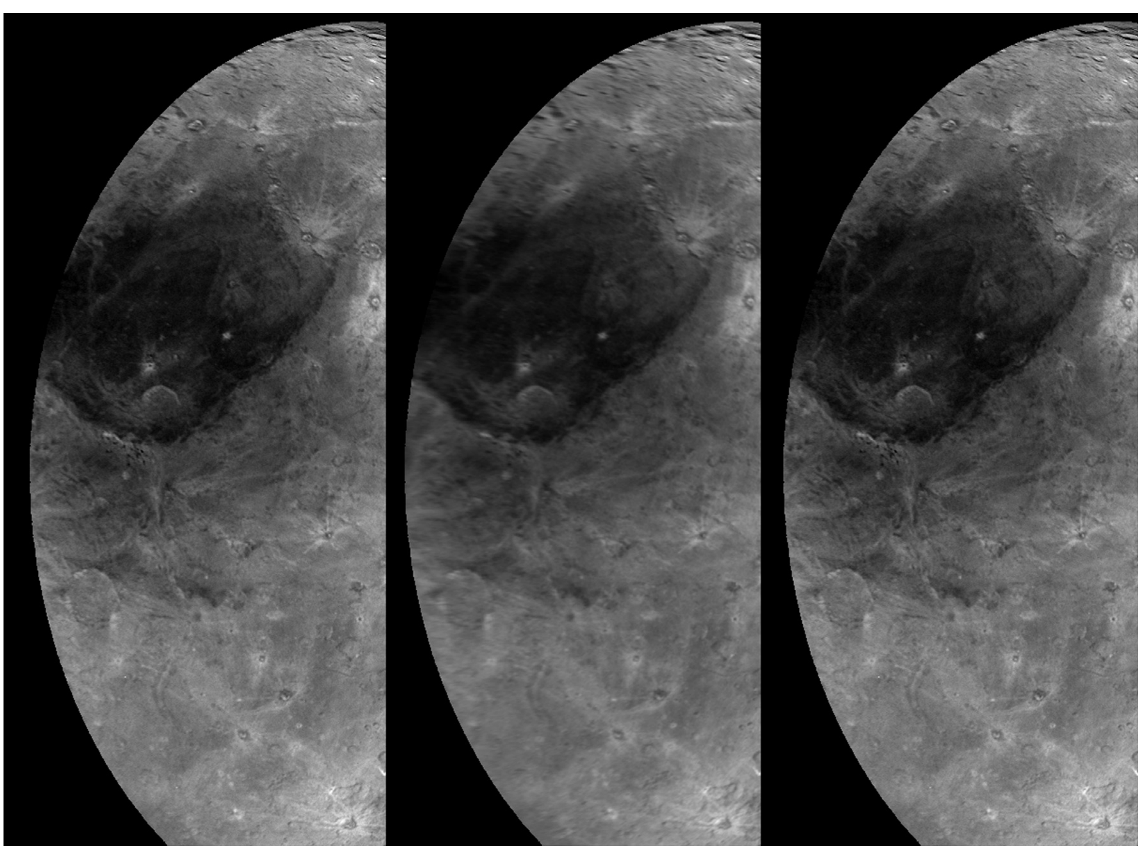

Fig. 15. (*continued*)

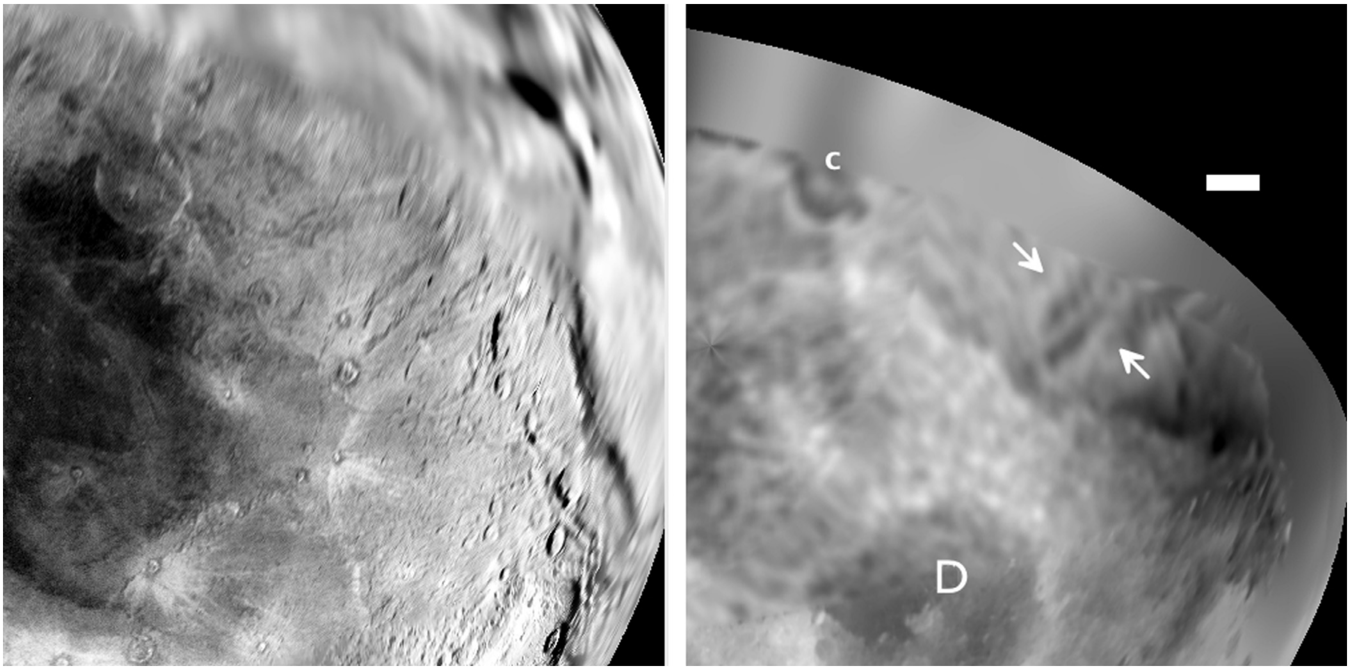

Fig. 16. Section of global color mosaic (left) and DEM (right) showing terrains along the outer margin of Mordor Macula between 40° and 140° longitude. Unusual double linear troughs are highlighted between the white arrows. Two craters (Dorothy, D, and an unnamed crater, c) form interruptions in the circular dark deposit of Mordor Macula (at left). Orthographic projection with north pole at center left. Scene is ~650 km across; north pole is at center left; scale bar is 50 km. Topographic range shown is −14 to +6 km.

elevations of the two terrains are even more divergent, with Vulcan Planitia lying > 2.5 km lower than Oz Terra by this measure, reflecting the difference between the Vulcan plains and the top surfaces of the broken crustal blocks within Oz. Regardless of exactly how and where the two terrains are measured, it is clear that their topography is complex and that Vulcan Planitia lies 1–3 km below Oz Terra as units but up to 6 km at their extremes.

The new (partial) global topographic maps of Charon (this report), ice-enriched dwarf planet Ceres (e.g., Preusker et al., 2016; Park et al., 2016), and the mid-sized icy moons of Saturn and Uranus (Schenk et al., 2018b) offer a first opportunity to compare the topographic properties of mid-sized icy bodies as a class (Fig. 20). Topographic data are available for 75–100% of the surfaces of the saturnian mid-sized moons, for ~30–40% of the 3 Uranian moons, and globally for Ceres (Fig. 20), and are referenced to the triaxial ellipsoidal figure of each body.

Topographic amplitude on Charon is the greatest observed on a mid-sized icy body other than Iapetus (Fig. 20). The 5 inner moons of Saturn, although very rugged on a local scale due to overlapping craters, are globally much more “relaxed” than either Charon or Iapetus (Schenk et al., 2018a). These inner moons also have a symmetric unimodal topographic signature except for two minor features: a bump at −6 km for Tethys representing the 45-km-diameter Odysseus impact, and a bump at −500 m on Enceladus representing the contribution from several 100-km scale dimples on the surface (Schenk and McKinnon, 2009). The lower amplitude topographic signature of the inner Saturn moons has been interpreted as an indication of the erasure of the signature of ancient accretional processes or heavy bombardment which apparently remains visible on Iapetus (Schenk et al., 2018a).

The three uranian satellites for which we have topographic signatures are intermediate in global ruggedness between Charon and the inner saturnian moons (Fig. 20). Their hypsograms are also more complex and more closely resemble the skewed shape of Charon's hypsogram (Fig. 20b). A bump at −1.5 km in the Ariel hypsogram probably reflects the troughs between the broken blocks on Ariel, potentially analogous to the breakup of Charon's crust, though the hypsogram of that moon is narrower than on Charon. The hypsogram of Titania is broadly similar in shape to Charon (Fig. 20b). This is likely a coincidence as Titania is a more heavily cratered body, though its icy shell is also disrupted by several large walled troughs (Croft and Soderblom, 1991). Evidence on Titania for geologic activity, topographic relaxation, or resurfacing is more limited than either Miranda or Ariel, suggesting limited hearting or a colder interior capable of retaining some topographic variations.

Voyager imaging for both Umbriel and Oberon, both of which are heavily cratered, is insufficient to permit DEM production, but several limb profiles were generated (Thomas et al., 1988). These data show that the topography of Oberon (where profiled) is broadly comparable to Titania with variations of relief of ± 3 km (excluding the 11-km high mountain. Umbriel is more rugged with variations in relief of ± 5 km locally. These data are consistent with the inferences gathered from the other three moons above that the Uranian moons are consistently more rugged than the 5 inner saturnian moons.

Curiously, the shape of the hypsogram for Charon is rather similar to that of Ceres (Preusker et al., 2016; Park et al., 2016), except that the low-elevation wing of the hypsogram of Ceres is not as deep as on Charon (Fig. 21) due to the lack of Charon-style deep troughs on Ceres. This is consistent with indications from viscous relaxation studies that the outer layers of Ceres are stiffer than expected for a pure-ice outer shell (e.g., Bland et al., 2016) and able to retain more of the long-wavelength topographic signature (e.g.,Fu et al., 2017) than the inner saturnian moons (Schenk et al., 2018a). Ceres topography is dominated by impact cratering and by several large-scale cryptic (possibly impact-related) depressions across its surface; whereas Charon is dominated by the topography of the breakup of its outer layers into large blocks separated by deep troughs and by the vast plains of Vulcan Planitia.

5.2. Origins of major morphologic and topographic units on Charon

The topography of the broken terrains of Oz Terra indicates that the icy shell of Charon has been broken into large crustal blocks (Moore et al., 2016; Beyer et al., 2017; Robbins et al., 2017), presumably due to global or regional extensional stresses. This could be due to a few

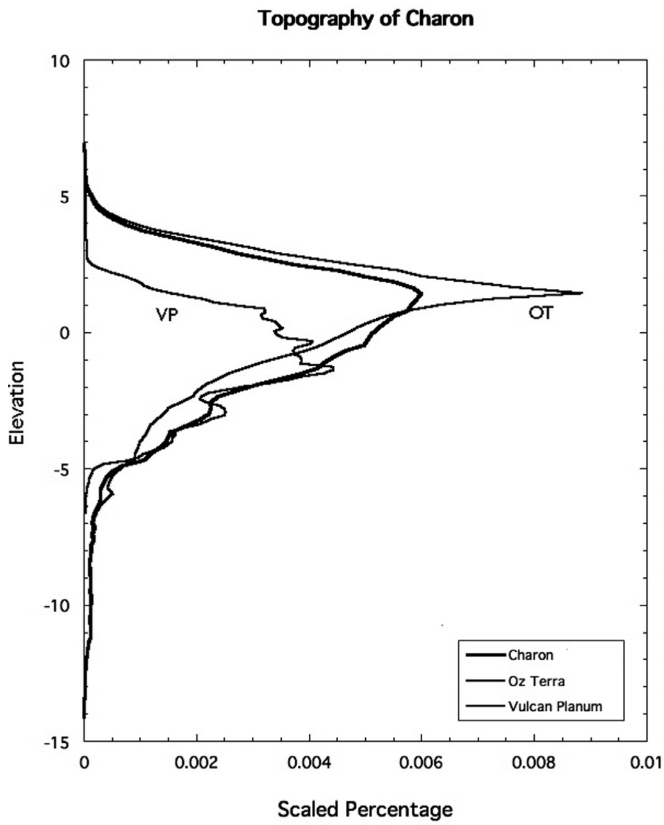

Fig. 17. Hypsograms of topography across the mapped DEMs of Charon and its two major terrain units. OT is Oz Terra data and VP is Vulcan Planitia data. Heavy curve is for all Charon terrains combined. Data are from Fig. 3. Low-resolution approach DEM data were excluded from hypsograms.

percent of global expansion, related to global cooling or perhaps freezing of a global water layer in the interior. Although a simple volcanic origin for Vulcan Planitia has been proposed and remains plausible (e.g., Moore et al., 2016), the break-up of Oz Terra, the tilted blocks along the northern border of Vulcan Planitia and the isolated massifs within (Figs. 9 and 12) suggest that rather than simple volcanic resurfacing by viscous melts of icy composition, we are instead seeing the foundering of crustal blocks (see also Beyer et al., 2018 for extended discussion), and subsequent replacement by icy materials that were originally beneath them. In this hypothesis, the isolated massifs are the visible remains of blocks that are almost but not quite subsumed. The converging curved troughs seen in some locations (Figs. 12 and 13) could be areas where the topmost portions of the crustal blocks have indeed foundered below the surface, leaving convergence 'suction ripples' where viscous material has covered them, much as large stones dropped into viscous mud can leave disturbances on the surface where they foundered. If correct, the plains of Vulcan Planitia could be interpreted as the exposed interior of Charon that has vertically replaced or covered the foundered blocks, consistent with the high viscosity of the plains inferred from the deep moats bordering Vulcan Planitia and the mountains scattered within it. If large blocks of Charon's ancient crust did indeed founder it would imply that a density inversion formed in the outer layers of this moon, with the outer layers acquiring a lower density than the interior. The origins of Vulcan Planitia are the subject of ongoing study (e.g., Beyer et al., 2018), but the topographic characteristics described above provide key constraints on its emplacement.

The breakup of Oz Terra into large blocks many tens to hundreds of kilometers wide by troughs tens of kilometers across is unusual in the outer solar system. The closest analog may be the breakup of large sections of the icy shell of Ariel into 40-to-200-km-wide blocks by linear troughs 3–5 km deep (e.g., Croft and Soderblom, 1991; Peterson et al., 2015) (Fig. 18). Most of the blocks are lightly cratered and flat-topped but a few blocks are also tilted (Figs. 18 and 19), perhaps in a manner similar to those along the southern margin of Oz Terra (Fig. 9). Whether any of Ariel's large blocks have foundered is unknown as 60% of the surface was unresolved or in darkness. With a few exceptions, the troughs between the blocks on Ariel have been resurfaced by smooth plains interpreted as volcanic (e.g., Croft and Soderblom, 1991), perhaps ammonia-hydrate in composition (Schenk, 1991). These resurfaced troughs may be analogous to the plains of Vulcan Planitia. In contrast, smooth plains materials do not fill most of the troughs within

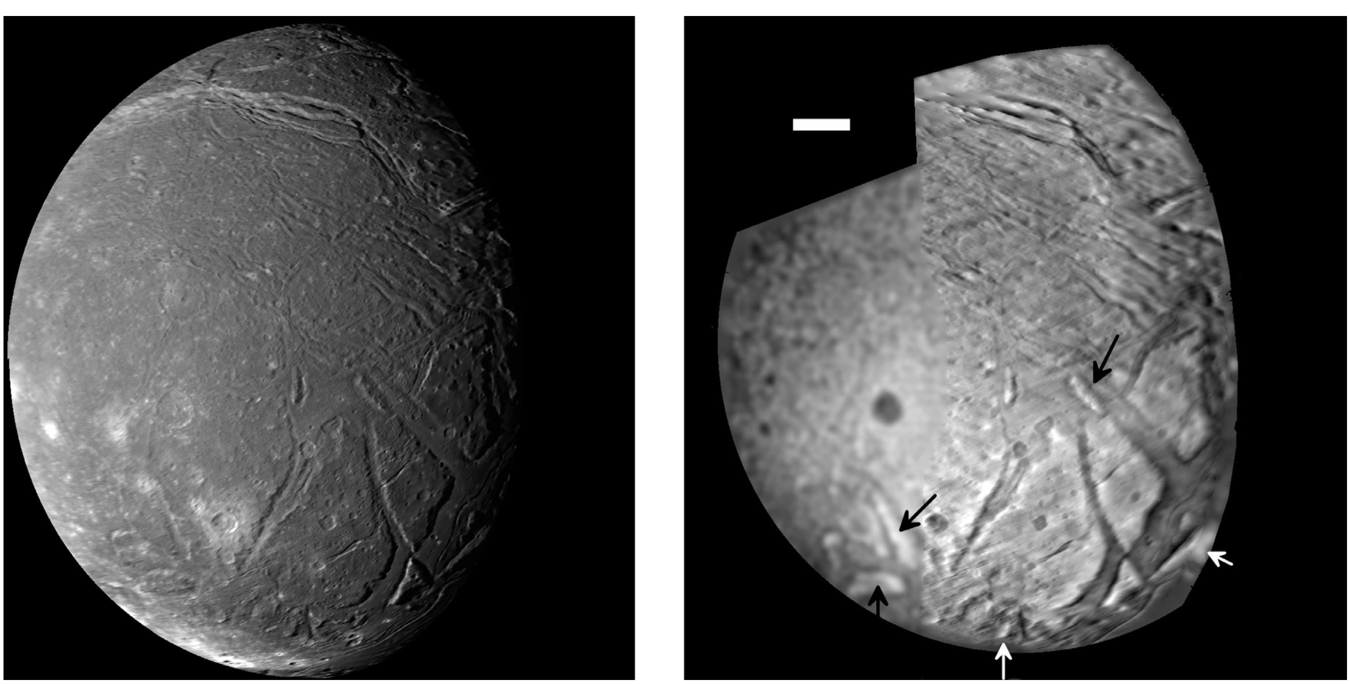

Fig. 18. Global mosaic (left) and DEM (right) for the Uranian moon Ariel. Disrupted crustal blocks are evident at lower right, and tilted blocks at lower left (black and white arrows) which are even more evident in the stereo images. Orthographic projection; south pole at left center; scale bar is 50 km.

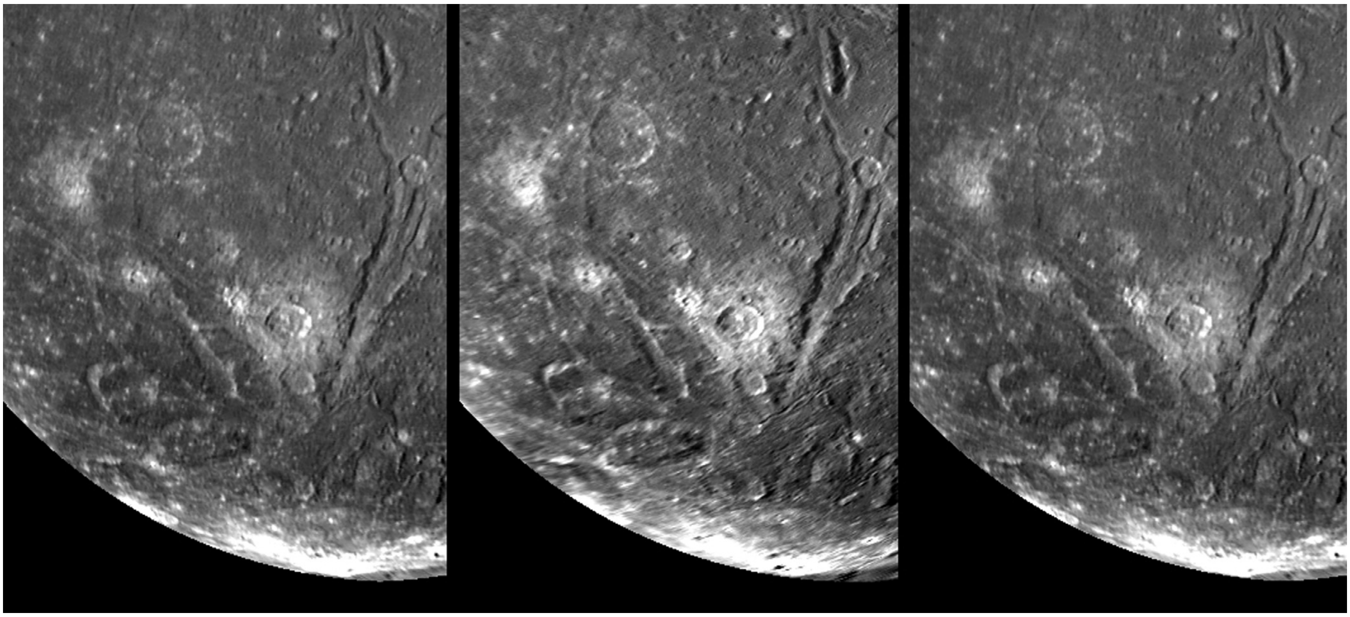

Fig. 19. Stereo pair of angular and tilted crustal blocks on Uranian icy moon Ariel. Area shown is from lower left of Fig. 18. The best evidence for tilted blocks is in the bottom half of frame. Images are at resolutions of 1.0 and 1.25 km/pixel. Figure format allows user to view in either wall-eyed mode (left-center) or cross-eyed mode (center-right). Red-blue anaglyph version of this figure is available in Supplementary Fig. 3.

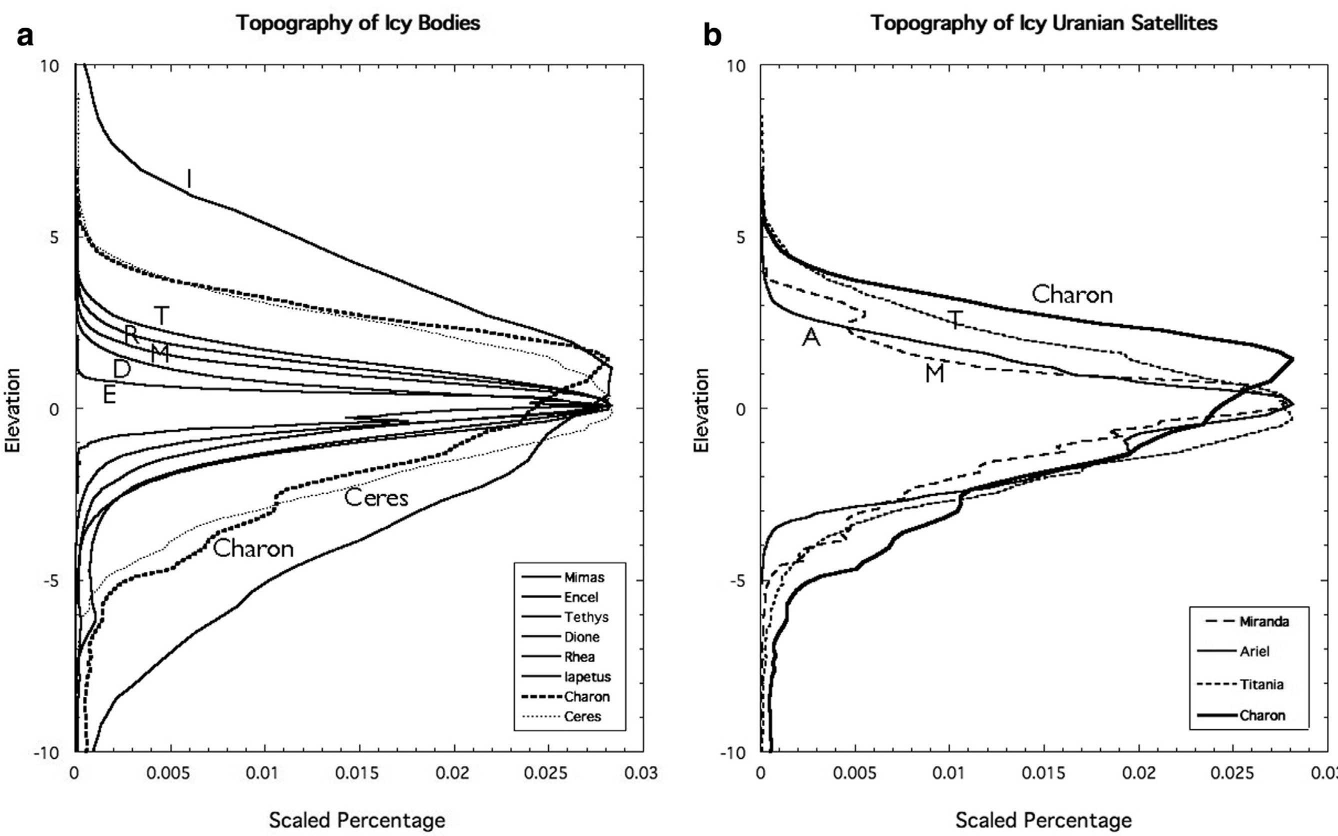

Fig. 20. (a) Hypsogram of topography for mid-sized icy bodies, comparing Charon (heavy line) and the icy moons of Saturn. Outermost solid line is Iapetus (greatest amplitude) and innermost or flattest is Enceladus. (b) Hypsogram of topography for mid-sized icy bodies, comparing Charon (heavy line) and the icy moons of Uranus. In all cases, topography is referenced to the mean triaxial ellipsoid of each body in order to compare deviations from this first-order shape.

Oz Terra on Charon, perhaps because they never widened or deepened to the degree observed on Ariel or the materials involved were too viscous.

The preservation of such a high degree of relief on Charon, including within the disrupted terrains of Oz Terra and despite the evidence for widespread resurfacing to the south in Vulcan Planitia, indicates that heat flow within the icy shell was not sufficient to erase the deep relief observed, or that any major heating events occurred before these geologic events. It also indicates that the icy shell of Charon must be dominated rheologically by relatively stiff material

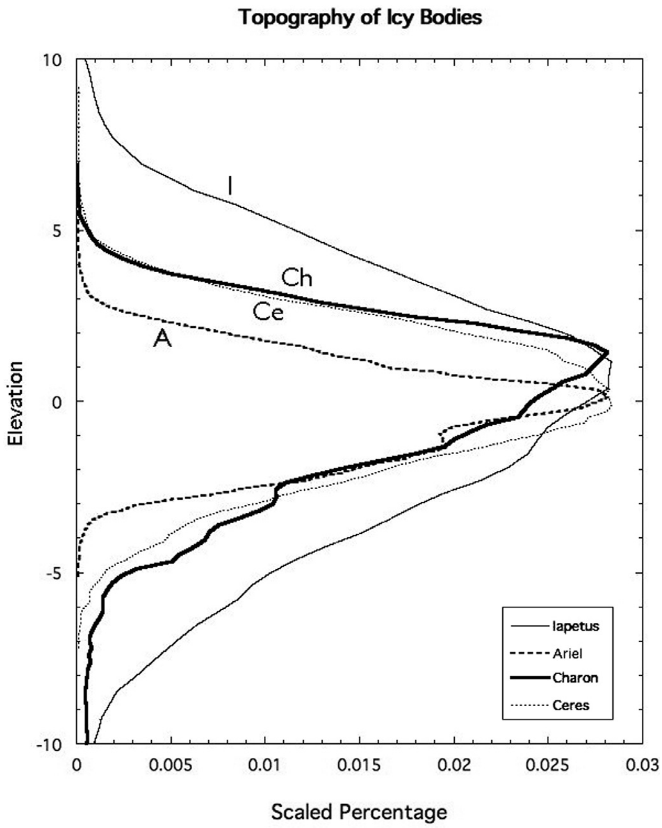

Fig. 21. Hypsograms of several mid-sized icy bodies, including Charon. This graph highlights several key comparisons, including Ceres (thin dashed line), saturnian moon Iapetus (outer solid line), the most rugged of icy mid-sized bodies, Uranian moon Ariel (heavy dashed line), and Charon (heavy line). Data for Ceres from Preusker et al. (2016) and Park et al. (2016).

such as water ice (e.g., Beyer et al., 2017). The rugged topographic signature of Charon appears due largely to the break-up of northern terrains and the emplacement of Vulcan Planitia, as the signatures of large ancient degraded impact structures evident in the topography of Iapetus are not observed on Charon. Rather it is the incomplete breakup and apparent foundering of large sections of the outer layers of Charon that dominates this moon geologically (Moore et al., 2016; Beyer et al., 2017; Robbins et al., 2017) and topographically.

Acknowledgments

We thank Brian Fessler and the IT staff at the Lunar and Planetary Institute, Houston, for their programing and computer support. We also thank the New Horizons navigation, sequencing, and science teams for their successful design and execution of these challenging observations. This work was supported by NASA's New Horizons project.

Supplementary materials

Supplementary material associated with this article can be found, in the online version, at doi:10.1016/j.icarus.2018.06.010.

References

Acton, C., Bachman, N., Diaz Del Rio, J., Semenov, B., Wright, E., Yamamoto, Y., 2011. SPICE: a means for determining observation geometry. In: EPSC-DPS Joint Meeting 2011, held 2–7 October 2011 in Nantes, France, pp. 32. http://meetings.copernicus.org/epsc-dps2011.

Archinal, B.A., A'Hearn, M.F., Bowell, E., Conrad, A., Consolmagno, G.J., Courtin, R., Fukushima, T., Hestroffer, D., Hilton, J.L., Krasinsky, G.A., Neumann, G., Oberst, J., Seidelmann, P.K., Stooke, P., Tholen, D.J., Thomas, P.C., Williams, I.P., 2011a. Report of the IAU working group on cartographic coordinates and rotational elements: 2009. Celestial Mech. Dyn. Astron. 109, 101–135. https://doi.org/10.1007/s10569-010-9320-4.

Archinal, B.A., A'Hearn, M.F., Conrad, A., Consolmagno, G.J., Courtin, R., Fukushima, T., Hestroffer, D., Hilton, J.L., Krasinsky, G.A., Neumann, G., Oberst, J., Seidelmann, P.K., Stooke, P., Tholen, D.J., Thomas, P.C., Williams, I.P., 2011b. Erratum to: reports of the IAU working group on cartographic coordinates and rotational elements: 2006 & 2009. Celestial Mech. Dyn. Astron. 110, 401–403. https://doi.org/10.1007/s10569-011-9362-2.

Beyer, R.A., et al., 2017. Charon tectonics. Icarus 287, 161–174. https://doi.org/10.1016/j.icarus.2016.12.018.

Beyer, R.A., et al., 2018. The nature and origin of Charon's smooth plains. In prep.

Bland, M., Raymond, C.A, Schenk, P.M., Fu, R.R., Kneissl, T., Pasckert, J.H., Hiesinger, H., Preusker, F., Park, R.S., Marchi, S., King, S.D., Castillo-Rogez, J.C., Russell, C.T., 2016. Composition and structure of the shallow subsurface of Ceres revealed by crater morphology. Nature Geosci. 9, 538–542. https://doi.org/10.1038/ngeo2743.

Bray, V., Schenk, P., 2015. Pristine impact crater morphology on Pluto - Expectations for New Horizons. Icarus 246, 156–164.

Buczkowski, D.,and25others, 2016. The geomorphology of Ceres. Science 353. https://doi.org/10.1126/science.aaf4332.

Cheng, A.F., et al., 2008. Long-range reconnaissance imager on New Horizons. Space Sci. Rev. 140, 189–215. https://doi.org/10.1007/s11214-007-9271-6.

Collins, G., McKinnon, W., Moore, J., Nimmo, F., Pappalardo, R., et al., 2010. Tectonics of the outer planet satellites. In: Schultz, RA, Watters, TR (Eds.), Planetary Tectonics. Cambridge Univ. Press, Cambridge, pp. 264–350.

Cook, A.C., Oberst, J., Roatsch, T., Jaumann, R., Acton, R.C., 1996. Clementine imagery: selenographic coverage for cartographic and scientific use. Planet. Space Sci. 44 (10), 1135–1148. https://doi.org/10.1016/S0032-0633(96)00061-X.

Cook, J.C.,and21co-authors, 2018. Composition of Pluto's small satellites: analysis of New Horizons spectral images. Icarus submitted.

Croft, S., Soderblom, L., 1991. Geology of the Uranian Satellites. In: Matthews, Bergstrahl, Miner (Eds.), Uranus, pp. 561–628.

Dalle Ore, C.,and10co-authors, 2018. Ices on Charon: distribution of H_2O and NH_3 from New Horizons LEISA observations. Icarus 300, 21–32. https://doi.org/10.1016/j.icarus.2017.08.026.

De Sanctis, M.,26others, 2016. Bright carbonate deposits as evidence of aqueous alteration on (1) Ceres. Nature 536, 54–57.

Durham, W.B., Prieto-Ballesteros, O., Goldsby, D.L., Kargel, J.S., 2010. Rheological and thermal properties of icy materials. Space Sci. Rev. 153, 273–298.

Fu, R.,and12others,, 2017. The interior structure of Ceres as revealed by surface topography. Earth Planet. Sci. Lett. 6, 153–164.

Grundy, W.M.,and33co-authors, 2016a. Surface compositions across Pluto and Charon. Science 351, 1283.

Grundy, W.M., et al., 2016b. The formation of Charon's red poles from seasonally cold-trapped volatiles. Nature 539, 7627, 65–68. https://doi.org/10.1038/nature19340.

Kargel, et al., 1991. Rheological properties of ammonia-water liquids and crystal-liquid slurries: planetological applications. Icarus 89, 93–112.

Lucy, L.B., 1974. An iterative technique for the rectification of observed distributions. Astron. J. 79, 745. https://doi.org/10.1086/111605.

McKinnon, W., 2012. Where did Ceres accrete? Asteroids Comets Meteor abstr. 6475.

Moore, J.M., et al., 2016. The geology of Pluto and Charon through the eyes of New Horizons. Science 351, aad7055, 1284–1293. https://doi.org/10.1126/science.aad7055.

Moore, J., and 11 others, 2017. Sublimation as a landform-shaping process on Pluto. Icarus 287, 320–333.

Moore, J., and 24 others, 2018. Bladed terrain on Pluto: Possible origins and evolution. Icarus 300, 129–144.

Nimmo, F., et al., 2017. Mean radius and shape of Pluto and Charon from New Horizons images. *Icarus* 287, 12–29.

Park, R., and 14 others, 2016. A partially differentiated interior for (1) Ceres deduced from its gravity field and shape. Nature 537, 515–517.

Peterson, A., Nimmo, F., Schenk, P., 2015. Elastic thickness and heat flux estimates for the uranian satellite Ariel,. Icarus 250, 116–122.

Preusker, F., and 10 others, 2016. Dawn at Ceres - shape model and rotational state. In: 47th Lunar Planet. Sci. Conf., abstr. pp. 1903.

Reuter, D.C., et al., 2008. Ralph: a visible/infrared imager for the New Horizons Pluto/Kuiper Belt Mission. Space Sci. Rev. 140, 129–154. https://doi.org/10.1007/s11214-008-9375-7.

Robbins, S.J., et al., 2017. *Geologic map of* New Horizons*' encounter Hemisphere of Charon*. In: *III*. Lunar & Planet Sci. Conf. 48 Abstract #1231.

Robbins, S., and 26 others, 2018. submitted, ICARUS, Geologic Landforms and Chronostratigraphic History of Charon as Revealed by a Hemispheric Geologic Map.

Richardson, W.H., 1972. Bayesian-based iterative method of image restoration. J. Opt. Soc. Am. 62, 55–59.

Schenk, P.M., 1991. Ganymede and Callisto: Complex crater morphology and formation processes on icy satellites. J. Geophys. Res. 96, 15,635–15,664.

Schenk, P.M., Bulmer, M.H., 1998. Origin of mountains on Io by thrust faulting and large-scale mass movements. Science 279, 1514–1518.

Schenk, P., McKinnon, W., 2009a. One-hundred-km-scale basins on Enceladus: evidence for an active ice shell. Geophys. Res. Lett. 36 CiteID L16202.

Schenk, P.M., Pappalardo, R.T., 2004. Topographic variations in chaos on Europa: implications for diapiric formation. Geophys. Res. Lett. 31 L16703.

Schenk, P., McKinnon, W., 2009b. One-hundred-km-scale basins on Enceladus: evidence for an active ice shell. Geophys. Res. Lett. 36 CiteID L16202.

Schenk, P., White, O., Byrne, P., Moore, J., 2018a. Geology of Saturn's Other Icy Moons, in Enceladus and the Icy Moons of Saturn. University of Arizona Press in press.

Schenk, P.,and10others, 2018b. Basin, fractures and volcanoes: global cartography and topography of Pluto from New Horizons. Icarus submitted.
Singer, K., et al., 2017. Impact craters on Pluto and Charon and evidence for a deficit of small. Kuiper Belt Objects submitted.
Stern, S.A., et al., 2015. The Pluto system: initial results from its exploration by New Horizons. Science 350, aad1815. https://doi.org/10.1126/science.aad1815.
Thomas, P., 1988. Radii, shapes, and topography of the satellites of Uranus from limb coordinates. Icarus 73, 427–441.
U.S. Geological Survey, 2017. Integrated Software for Imagers and Spectrometers (ISIS). . http://isis.astrogeology.usgs.gov.
White, O.L, Schenk, P.M., Dombard, A.J., 2013. Impact basin relaxation on Rhea and Iapetus and relation to past heat flow. Icarus 223, 699–709.
White, O.L., Schenk, P.M., Bellagamba, A., Grimm, A., Dombard, A.J., Bray, V., 2017. Impact crater relaxation on *Dione* and *Tethys* and relation to past heat flow. Icarus 288, 27–52.
Zangari, A., 2015. A meta-analysis of coordinate systems and bibliography of their use on Pluto from Charon's discovery to the present day. Icarus 246, 93–145. https://doi.org/10.1016/j.icarus.2014.10.040.